Author Manuscript

Author Manuscript

Author Manuscript

Author Manuscript

HHS Public Access

Author manuscript

Neuron. Author manuscript; available in PMC 2021 March 18.

Published in final edited form as:

Neuron. 2020 March 18; 105(6): 1094–1111.e10. doi:10.1016/j.neuron.2019.12.027.

Estimation of Current and Future Physiological States in Insular Cortex

Yoav Livneh[1], **Arthur U. Sugden**[1], **Joseph C. Madara**[1], **Rachel A. Essner**[1,2], **Vanessa I. Flores**[1], **Lauren A. Sugden**[3], **Jon M. Resch**[1], **Bradford B. Lowell**[1,2,*], **Mark L. Andermann**[1,2,4,*]

[1]Division of Endocrinology, Diabetes and Metabolism, Beth Israel Deaconess Medical Center, Harvard Medical School, Boston, MA, USA, 02215

[2]Program in Neuroscience, Harvard Medical School, Boston, MA, USA, 02115

[3]Department of Mathematics and Computer Science, Duquesne University, Pittsburgh, PA, 15232

[4]Lead contact

Summary

Interoception, the sense of internal bodily signals, is essential for physiological homeostasis, cognition, and emotions. While human insular cortex (InsCtx) is implicated in interoception, the cellular and circuit mechanisms remain unclear. We imaged mouse InsCtx neurons during two physiological deficiency states – hunger and thirst. InsCtx ongoing activity patterns reliably tracked the gradual return to homeostasis, but not changes in behavior. Accordingly, while artificial induction of hunger/thirst in sated mice via activation of specific hypothalamic neurons (AgRP/SFO^{GLUT}) restored cue-evoked food/water-seeking, InsCtx ongoing activity continued to reflect physiological satiety. During natural hunger/thirst, food/water cues rapidly and transiently shifted InsCtx population activity to the future satiety-related pattern. During artificial hunger/thirst, food/water cues further shifted activity *beyond* the current satiety-related pattern. Together with circuit-mapping experiments, these findings suggest that InsCtx integrates visceral-sensory inputs regarding current physiological state with hypothalamus-gated amygdala inputs signaling upcoming ingestion of food/water, to compute a prediction of future physiological state.

Graphical Abstract

[*]**Correspondence:** blowell@bidmc.harvard.edu; manderma@bidmc.harvard.edu.

Author contributions

YL, BBL and MLA designed the experiments and wrote the manuscript. YL performed imaging, feeding and drinking studies, and data analyses. AUS assisted with data analysis and provided conceptual input. AUS and LAS developed the AODE classifier. YL, VIF, and RAE performed circuit mapping and drinking studies. JCM performed slice electrophysiology. JMR assisted with studies of water consumption and provided conceptual input.

Publisher's Disclaimer: This is a PDF file of an unedited manuscript that has been accepted for publication. As a service to our customers we are providing this early version of the manuscript. The manuscript will undergo copyediting, typesetting, and review of the resulting proof before it is published in its final form. Please note that during the production process errors may be discovered which could affect the content, and all legal disclaimers that apply to the journal pertain.

Declaration of Interests

The authors declare no competing interests.

Author Manuscript Author Manuscript Author Manuscript Author Manuscript

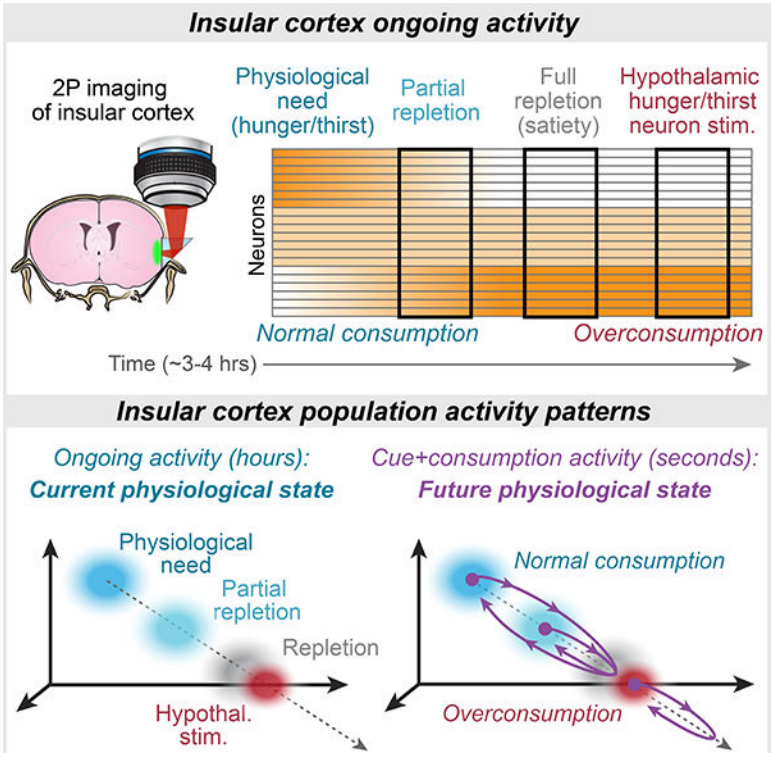

eTOC Blurb:

Livneh et al. find that slow changes in ongoing population activity patterns in insular cortex reflect physiological need states, independent of behavior and hypothalamic hunger/thirst neurons. Food/water cues and consumption drive population activity to transiently “simulate” a future satiety state.

Introduction

Interoception, the sense of the physiological condition of the body (Craig, 2003), involves sensing and integrating various signals related to heart rate, blood glucose levels, blood CO_2 levels, temperature, inflammation, and more (Craig, 2003; Critchley and Harrison, 2013; Gogolla, 2017; Saper, 2002). Insular cortex (InsCtx) is the main cortical site that performs the integration of these signals from brainstem and thalamic sensory pathways (Saper, 2002), and is thus considered to be a key hub for interoception.

InsCtx is thought to mediate the interoceptive aspects of numerous behaviors, from feeding and drinking to social behaviors. Furthermore, InsCtx is implicated in pathological conditions including eating disorders, obesity, anxiety, major depression and addiction (Barrett and Simmons, 2015; Critchley and Harrison, 2013; Frank et al., 2013; Garcia-Cordero et al., 2016; Gehrlach et al., 2019; Khalsa et al., 2018; Naqvi et al., 2014). However, the role of InsCtx in interoception remains unclear, as humans and rodents with lesioned/silenced InsCtx largely maintain habitual motivated behaviors such as eating and drinking (Livneh et al., 2017; Naqvi et al., 2014).

Author Manuscript Author Manuscript Author Manuscript Author Manuscript

Prevailing models suggest that InsCtx receives sensory information regarding changes in bodily physiology (e.g., following food or water deficits), and integrates this with external sensory cues, associated action plans, and expected outcomes (Contreras et al., 2007; Kusumoto-Yoshida et al., 2015; Livneh et al., 2017; Naqvi et al., 2014). In particular, such models implicate InsCtx in computing "interoceptive predictions" (Barrett and Simmons, 2015; Owens et al., 2018; Paulus et al., 2019; Quadt et al., 2018). Consistent with these active inference models, human and rodent InsCtx responds to salient predictive cues across different sensory modalities (Gardner and Fontanini, 2014; Kusumoto-Yoshida et al., 2015; Livneh et al., 2017; Vincis and Fontanini, 2016). In addition, human neuroimaging studies suggest that InsCtx represents physiological states, such as hunger and thirst (Egan et al., 2003; Meier et al., 2018; Tataranni et al., 1999).

Physiological need states, such as hunger and thirst, can serve as powerful models to study interoception. These states involve specific physiological deficits that are sensed via interoceptive signals, ultimately giving rise to a specific motivational drive that helps correct the deficiency (Augustine et al., 2018b; Gizowski and Bourque, 2018; Lowell, 2019; Sternson and Eiselt, 2017; Zimmerman et al., 2017). These motivational drives can be recapitulated artificially via activation of distinct, genetically defined populations of hypothalamic neurons, such as hunger-promoting neurons expressing agouti-related peptide (AgRP neurons), and thirst-promoting glutamatergic subfornical organ (SFO) neurons (Aponte et al., 2011; Betley et al., 2015; Chen et al., 2016; Krashes et al., 2011; Oka et al., 2015). For simplicity and brevity, we will refer to these neurons as "hunger neurons" or "thirst neurons", as they are thought to act both as sensors of physiological imbalances and as actuators of relevant behavioral and physiological counter-regulatory responses, including seeking and consummatory behaviors (Andermann and Lowell, 2017).

We recently developed a microprism-based method for cellular-resolution imaging of mid-posterior InsCtx in behaving mice (Livneh et al., 2017). We initially focused on hunger, and found that InsCtx neurons showed selective responses to food-predicting cues that were abolished following satiation, but restored following activation of AgRP neurons. Circuit mapping and pathway-specific manipulations defined a functionally relevant pathway linking AgRP neurons to InsCtx via paraventricular thalamus (PVT) and basolateral amygdala (BLA; Livneh et al., 2017). In the current study, we first asked whether these results generalized to thirst and water cues. We then considered whether InsCtx ongoing activity patterns represent distinct physiological states, and how these representations might be integrated with those encoding need-relevant predictive cues. Our results suggest the following model: first, information regarding learned cues signaling the availability of food/water is relayed to InsCtx via a PVT→BLA pathway, gated by hypothalamic hunger/thirst neurons. InsCtx activity then transiently shifts from a hypothalamus-independent estimate of current physiological state to a prediction of future physiological state.

Results

We examined thirst-dependent InsCtx responses to water-predicting cues using behavioral procedures we have previously used to examine hunger-dependent responses to food-predicting cues in InsCtx and other cortical areas (Burgess et al., 2016; Livneh et al., 2017).

Author Manuscript Author Manuscript Author Manuscript Author Manuscript

We trained water-restricted mice to perform an operant Go/No-Go visual discrimination task in which licking following presentation of three initially arbitrary visual cues leads to rewarding (water), aversive (1 M NaCl), or neutral outcomes (Fig. 1A). Well-trained thirsty mice quenched their thirst either by performing the task until voluntary cessation, or by drinking water continuously in the absence of visual cues (intake of ~0.5–1 mL in ~2–5 minutes). We operationally defined a quenched state by voluntary, sustained cessation of water consumption (Fig. 1B; Fig. S1A,D).

We imaged GCaMP6f-expressing layer 2/3 neurons in InsCtx via a microprism (Livneh et al., 2017) in mice performing this behavioral task (Fig. 1C; 1953 neurons in 12 fields-of-view [FOV] from 9 mice across thirsty and quenched states). As in previous studies, individual neurons could respond to the visual water cue, to onset of licking, or to water reward delivery (Fig. 1D; de Araujo et al., 2006; Gardner and Fontanini, 2014; Katz et al., 2001; Levitan et al., 2019b; Livneh et al., 2017; Samuelsen et al., 2012; Stapleton et al., 2006). The majority of neurons (~80%) responded to either the water cue and/or water reward consumption, and ~30% responded to at least one learned visual cue (Fig. 1E). Interestingly, neurons either activated or suppressed by the water cue were intermingled throughout mid-posterior InsCtx, with no clear topographic organization (Fig. S1B).

Average responses across sets of neurons, activated or suppressed by visual cues, were abolished after quenching of thirst (Fig. 1F). Most cue responsive neurons responded predominantly to the water cue in the thirsty state, with dramatically attenuated responses in the quenched state (Fig. 1G,H). Importantly, we verified that these results were not due to different arousal levels across thirsty and quenched states. To do so, we used moment-to-moment changes in pupil diameter as a proxy for changes in arousal (McGinley et al., 2015), following our previously established procedure (Fig. S1C; Livneh et al., 2017).

The sensation of thirst is affected not only by current fluid balance, but also by “subjective satiety” that accompanies anticipation of imminent restoration of homeostasis by fluid absorption (Augustine et al., 2018a; Gizowski and Bourque, 2018; Zimmerman et al., 2016). We thus compared datasets involving gradual quenching during tens of minutes of task engagement, to datasets collected immediately following rapid quenching via 2–5 minutes of continuous consumption (osmotic balance is restored after ~10 minutes; Mandelblat-Cerf et al., 2017). We found similar attenuation of water cue responses following both gradual and rapid quenching protocols (Fig. 1I).

In summary, thirst-dependent InsCtx responses to water cues and drinking are similar to hunger-dependent InsCtx responses to food cues and feeding (Livneh et al., 2017). We and others have previously shown that BLA inputs are necessary for InsCtx predictive cue responses in both hungry and thirsty states (Livneh et al., 2017; Samuelsen et al., 2012). However, it remained unclear whether BLA inputs to InsCtx played an “instructive” role (i.e., relaying learned cue-related information) and/or a “permissive” role (e.g., providing necessary tonic activity but not relaying cue information; Wolff and Olveczky, 2018). We next addressed this by recording the activity of BLA inputs to InsCtx.

Author Manuscript Author Manuscript Author Manuscript Author Manuscript

Thirst-Dependent Response Bias to Water Cues in BLA→InsCtx Axons

We expressed GCaMP6s in the BLA, and used the same microprism preparation to image the activity of BLA axons in InsCtx (Fig. 1J). We grouped together highly correlated signals from boutons belonging to the same axon (Fig. 1K; Supp. Video 1; Burgess et al., 2016).

We imaged a total of 257 axons in 5 FOVs from 3 mice across thirsty and quenched states (Fig. S1D). Single axons could respond to either the water cue, to onset of licking, and/or to water reward delivery (Fig. 1L), consistent with previous studies (Baxter and Murray, 2002; Beyeler et al., 2016; Grewe et al., 2017; Kyriazi et al., 2018; Lutas et al., 2019; Morrison and Salzman, 2010; Zhang and Li, 2018), and with the broad collateralization of BLA→InsCtx axons (Livneh et al., 2017). The vast majority of imaged axons (~91%) responded to either the water cue and/or water reward, while ~50% responded to learned visual cues (Fig. 1M).

Average visual responses across either activated or suppressed axons were abolished after quenching of thirst (Fig. 1N). Similar to InsCtx neurons, cue responsive BLA→InsCtx axons responded predominantly, and more strongly, to the water cue (Fig. 1O, S1E). These results were not due to different arousal levels across thirsty and quenched states (Fig. S1F; Livneh et al., 2017; Lutas et al., 2019). Similarly, BLA→InsCtx axons showed strong and selective food cue responses during a hungry state but not during a sated state (Fig. S1G–K). Together, these data support an “instructive role” (but do not exclude an additional “permissive role”) for BLA inputs in relaying motivationally relevant learned cues to InsCtx. In contrast, gustatory information and visceral information regarding physiological states are likely relayed to InsCtx via other pathways (Samuelsen et al., 2013; Saper, 2002).

Putative Representation of Thirst State in Ongoing InsCtx Activity

Throughout our experiments, we observed high levels of ongoing activity in InsCtx even when mice were not performing the behavioral task (i.e., during quiet waking periods; Fig. 2A; Supp. Video 2). This is consistent with the relatively high spiking rates in mouse InsCtx vs. other cortical regions (Kusumoto-Yoshida et al., 2015; Levitan et al., 2019b). Furthermore, some neurons had different levels of ongoing activity across thirsty and quenched states (Fig. 2A). Human neuroimaging studies show that InsCtx tracks slow variations in physiological states, including hungry vs. sated and thirsty vs. quenched states (Egan et al., 2003; Meier et al., 2018; Tataranni et al., 1999). We therefore wondered whether mouse InsCtx ongoing activity during the task (in between cue presentations) might reflect aspects of physiological state. In this case, task-evoked neural responses would occur on top of physiological state-dependent patterns of ongoing activity (Arieli et al., 1996). Alternatively, ongoing activity could reflect other variables such as arousal or motor actions (Musall et al., 2019; Salkoff et al., 2019; Stringer et al., 2019).

To test this, we used a generalized linear model (GLM) to quantify the proportion of InsCtx activity that could be explained by behavioral task-related events and arousal state (Fig. 2B; Driscoll et al., 2017; Ramesh et al., 2018). We modeled the activity of each neuron based on variables that describe task-related events (cue onset, licking, water reward, high salt-water punishment), as well as arousal and body/brain motion (pupil diameter, locomotion, and

Author Manuscript Author Manuscript Author Manuscript Author Manuscript

estimated lateral motion of the imaging plane). Interestingly, the GLM could predict activity well only in a small subset of InsCtx neurons (fractional deviance explained: 0.13 ± 0.003; n=1953 neurons from 9 mice; Fig. 2C). In primary visual cortex (V1) neurons, which exhibit lower ongoing firing rates, robust visual cue-evoked responses and strong sensitivity to arousal/locomotion (Andermann et al., 2013; Andermann et al., 2011; McGinley et al., 2015; Niell and Stryker, 2010), the fractional deviance explained by these factors was two-fold higher during the same task (0.25±0.01; n=184 neurons from 3 mice; Fig. 2C).

To directly examine InsCtx ongoing activity during gradual quenching of thirst, we focused on inter-trial interval (ITI) periods in between cue presentations. We minimized any residual effects of task-related activity by concatenating the last 3 sec of ITI periods, and only including ITIs that followed blank trials and aversive/neutral cue trials, for which mice did not respond (i.e., “correct rejections”; Fig. 2D). Furthermore, we removed epochs that contained any licking. Notably, each selected ITI period occurred at least 13–25 sec after the previous water reward (see Methods).

We examined whether the pattern of InsCtx population activity during these concatenated ITI periods (referred to henceforth as “ongoing activity”) tracked hydration state during the visual discrimination task (n=153±25 neurons per FOV, 9 FOVs from 7 mice). Indeed, during a thirsty state, some neurons exhibited high ongoing activity that then decreased as mice became quenched, while other neurons exhibited the opposite trend (Fig. 2E–F).

Using principle component analysis (PCA), we found that InsCtx activity patterns during thirsty states were separable from those during quenched states (Fig. 2G, *left*, Fig. S2A). Moreover, these patterns and their separability were consistent across days, as demonstrated by projecting data from a given session onto principle components from the previous day’s session (Fig. 2G, *right*). To quantify the separability of ongoing activity patterns, we took a classification-based approach. We used an Averaged One-Dependence Estimator (AODE) classifier, an extension of the Naïve Bayes classifier that also accounts for pairwise correlations between neurons (Sugden et al., 2018; Webb et al., 2005). Using this approach and within-day cross-validation, we could readily classify thirsty vs. quenched states from ongoing activity. Strikingly, classification was high and above chance for all datasets, even when we trained the classifier on data from a given day and applied it to data acquired the following day (Fig. 2H).

Classification of thirsty/quenched states across days went to chance levels following random temporal shuffling of population activity patterns across the session (Fig. S2B). Interestingly, while shuffling of neuron identities also reduced across-day classification in 9/9 cases, identity-shuffled population data still classified thirst state above chance levels in some cases (Fig. S2B). This suggests that a relatively large fraction of the population contained relevant information. Indeed, when we systematically omitted neurons, classification was reduced to chance levels only after omitting the most informative 40% of neurons (i.e., those whose activity differed most across states; Fig. S2C). Furthermore, pairwise correlations were not essential for classification of thirsty/quenched states, as classification was similar using a Naïve Bayes classifier (Fig. S2D). Importantly, the actual *pattern* of activity across the population was essential, as thirsty/quenched states could not

Author Manuscript Author Manuscript Author Manuscript Author Manuscript

be classified from a single time course of activity averaged across the population (Fig. S2E). Notably, thirsty/quenched state classification was not a result of spatial organization, as neurons with increases or decreases in ongoing activity between thirsty and quenched states were spatially intermingled throughout mid-posterior InsCtx with no clear topographic organization (Fig. 2I).

InsCtx Ongoing Activity Reflects Physiological State Rather Than Arousal or Behavioral State

Differences in InsCtx ongoing activity between thirsty and quenched states could potentially reflect differences in physiological state (e.g., systemic osmolarity) or differences in behavioral state (e.g., arousal, motivation, etc.). We next tested these interpretations.

The above analyses focused on across-day classification of thirsty vs. quenched epochs. We therefore began by assessing how gradual changes in ongoing activity patterns relate to changes in behavior across the entire recording session using across-day classification (Day 2 data, Day 1 classifier). Surprisingly, ongoing activity could transition to a quenched state long before any overt change in task engagement (Fig. 3A,S3A). Specifically, in 7/9 cases, ongoing activity transitioned to a quenched state while mice were still at peak performance, reflected by a similarly high rate of correct responses to the water cue pre- vs. post-transition (100±3% vs. 100±0%, $p = 0.5$, paired t-test), and a similarly low rate of incorrect responses to other cues (0±0% vs. 4±3%, $p = 0.5$). The transition in ongoing activity pattern to a quenched state occurred 3–25 min *before* any drop in task performance (Fig. 3B), and was highly predictive of the eventual drop in task performance (Fig. 3C), across a range of analysis parameters (Fig. S3B). We also observed similar effects using an alternative method involving a scalar estimate of pattern similarity (Fig. S3C).

To more directly test whether InsCtx ongoing activity represents physiological states or related internal states such as arousal or motivation, we asked whether ongoing activity dynamics (as reflected in dynamics of classifier state estimation) could be predicted by a combination of four parameters: (1) cumulative amount of water consumed (coarsely reflecting hydration), (2) pupil diameter (a proxy for arousal; McGinley et al., 2015), and (3,4) lick response latency and lick rate on the most recent rewarded trial (reflecting motivational levels; Berditchevskaia et al., 2016; Fig. 3D). A linear combination of all four parameters effectively captured ongoing activity dynamics across the session (R^2=0.8±0.04; Fig. 3E, see example in Fig. S3D,E). We then systematically omitted different parameters and found that the only essential parameter for accurately predicting ongoing activity dynamics was the cumulative amount of water consumed. The omission of this parameter reduced the explained variance in 9/9 cases (R^2=0.56±0.05). Omission of any of the other parameters did not substantially affect explained variance (Fig. 3E).

We also considered the possibility that ongoing activity reflected time elapsed in the session (Wittmann, 2013). In a subset of mice (n=6), we decoupled time elapsed in the session from amount of water consumed by also imaging during ten-minute periods of forced task disengagement (no cues, no water delivery, and excluding time-points with licking; Fig. S3F) partway through the training session. Ongoing activity was similar before and after these periods (Fig. S3G), suggesting that the actual amount consumed – rather than time

Author Manuscript Author Manuscript Author Manuscript Author Manuscript

elapsed – drove the observed changes in ongoing activity. Interestingly, activity during these disengagement periods (which involved whisking, grooming and other so-called "spontaneous" behaviors) was in some cases different from ongoing activity during prior and subsequent task performance. This is consistent with recent evidence of correlations between neural activity and these "spontaneous" behaviors in almost all examined brain regions, including InsCtx (Stringer et al., 2019). Experiments involving artificial activation of hypothalamic thirst/hunger neurons or systemic injection of water provided additional confirmation that InsCtx ongoing activity does not reflect task engagement (see Fig. 6).

We next examined whether distinct patterns of ongoing activity in InsCtx reflect fluid deficiency (thirst) and caloric deficiency (hunger). We could readily classify InsCtx ongoing activity patterns during hungry vs. sated states in mice trained on an identical task but with cues predicting liquid food instead of water (data from Livneh et al., 2017), both within and across days (Fig. S3H). In contrast, training the classifier on *thirsty/quenched* states from one day resulted in poor classification of *hungry/sated* states from the following day (Fig. S3I). This suggests that InsCtx ongoing activity may differentiate between distinct deficiency states. Notably, we could not classify hungry/sated states from ongoing activity during the same task in two other cortical areas – V1 and postrhinal cortex (Fig. S3J; data from Burgess et al., 2016). Therefore, although some aspects of ongoing activity related to arousal and motor actions are ubiquitous throughout cortex (Allen et al., 2019; Musall et al., 2019; Salkoff et al., 2019; Stringer et al., 2019), reliable representations of physiological state may be more specific to a subset of areas including InsCtx.

The results presented thus far, together with our previous work involving hunger and satiety (Livneh et al., 2017), suggest that InsCtx neurons respond selectively to learned water cues or learned food cues when such cues are motivationally salient. Additionally, distinct physiological states associated with hunger or thirst are represented in patterns of InsCtx ongoing activity. Trans-synaptic tracing experiments suggest a potential connection between thirst-promoting neurons and InsCtx (Hollis et al., 2008). Furthermore, we previously demonstrated a pathway from hunger-promoting hypothalamic AgRP neurons to InsCtx via PVT→BLA (Livneh et al., 2017). In addition, BLA inputs provide learned water and food cue information to InsCtx (Figure 1, and Livneh et al., 2017). We therefore asked: do thirst-promoting neurons converge onto this same pathway? Do hypothalamic hunger and thirst neurons both regulate InsCtx responses to learned cues? Do these neurons affect representations of physiological states in InsCtx ongoing activity? In the following sections (Figures 4–6), we address these questions.

Convergence of Hypothalamic Thirst and Hunger Neurons on a Common Pathway to InsCtx

We first tested whether thirst-promoting hypothalamic neurons and AgRP neurons converge on the same pathway to gate InsCtx activity (Fig. 4A). We focused on glutamatergic neurons in SFO and median preoptic regions of the lamina terminalis (SFO^{GLUT} and $MnPO^{GLUT}$). SFO^{GLUT} neurons promote thirst (Betley et al., 2015; Oka et al., 2015) via projections to MnPO (Augustine et al., 2018a; Leib et al., 2017). Activation of $MnPO^{GLUT}$ neurons drives

Author Manuscript Author Manuscript Author Manuscript Author Manuscript

thirst when using a variety of genetic or activity-dependent methods to target them (Abbott et al., 2016; Augustine et al., 2018a; Leib et al., 2017; Marciante et al., 2019).

We confirmed that SFO^{GLUT} neurons send sparse projections to PVT, while $MnPO^{GLUT}$ neurons (labeled using vGLUT2-Cre or Nos1-Cre, which predominantly labels $vGLUT2^{+}$ neurons; Allen et al., 2017; Augustine et al., 2018a) send dense projections to PVT (Fig. 4B). We then used channelrohodopsin2 (ChR2)-assisted circuit mapping to test whether $MnPO^{GLUT}$ neurons converge on the PVT→BLA→InsCtx pathway. We expressed ChR2 in $MnPO^{GLUT}$ neurons and injected a retrograde tracer, CTB, in BLA. We then recorded light-evoked excitatory currents from CTB-labeled PVT→BLA neurons and found that 100% (41/41) received synaptic input from $MnPO^{GLUT}$ neurons (Fig. 4C). This suggests that many PVT→BLA neurons receive convergent input from both $MnPO^{GLUT}$ and AgRP neurons, as ~70% of PVT→BLA neurons also receive input from AgRP neurons (Livneh et al., 2017). Interestingly, a lower but substantial proportion of CTB^{-} PVT neurons (25/31, ~80%) also received synaptic input from $MnPO^{GLUT}$ neurons. The convergence of GABAergic “hunger neurons” and glutamatergic “thirst neurons” onto the same individual PVT→BLA neurons suggests a potential antagonism or competition between these two drives at the single-cell level (see Discussion).

Finally, we tested the potential importance of this pathway *in vivo*, by expressing ChR2 in $MnPO^{GLUT}$ neurons (using vGLUT2-Cre) and activating their terminals in PVT (Fig. 4D). This induced robust drinking (see also Allen et al., 2017; Leib et al., 2017), but not feeding (Fig. 4D). The induction of drinking might be partially attributable to activation of collateral projections that we observed in the paraventricular hypothalamus and lateral hypothalamus (LH; Fig. S4), consistent with recent reports of drinking-promoting LH neurons (Kurt et al., 2018). Together, these results suggest a potential convergence between hunger-and thirst-promoting hypothalamic neurons on a pathway to InsCtx (Fig. 4A).

Manipulations of Hypothalamic Hunger/Thirst Neurons Affect InsCtx Learned Cue Responses but Not Ongoing Activity

We next tested whether activation of thirst neurons would restore InsCtx cue responses and ongoing activity patterns to those observed in thirsty mice. Lamina terminalis structures are reciprocally connected but hierarchically organized (Augustine et al., 2018a). Because available Cre driver mouse lines do not necessarily exclusively label the thirst-related MnPO neurons, we used upstream SFO^{GLUT} neurons as an entry-point for artificial activation of the thirst circuitry (Augustine et al., 2018a; Leib et al., 2017). We used chemogenetics (hM3Dq) to artificially activate SFO^{GLUT} neurons, as previously described (Fig. 5A; Betley et al., 2015). We imaged InsCtx across natural thirsty and quenched states. We then injected the hM3Dq ligand clozapine-n-oxide (CNO) to activate SFO^{GLUT} neurons in quenched mice. Remarkably, after SFO^{GLUT} activation, all mice selectively licked to the water cue but withheld licking to other cues (Fig. 5B–D). Importantly, injection of CNO in the absence of hM3Dq expression did not induce drinking (Fig. S5A).

SFO^{GLUT} activation during a quenched state largely restored InsCtx cue responses to those observed during natural thirst (Fig. 5E; n=597 neurons from 4 mice). SFO^{GLUT} activation, but not control saline injections, also restored the InsCtx water cue response bias (Figs

Author Manuscript Author Manuscript Author Manuscript Author Manuscript

5F,S5B). InsCtx water cue responses following SFO^{GLUT} activation in quenched mice were similar to those during natural thirst in ~70% of neurons. This was comparable to the level of similarity of water cue responses across two consecutive sessions during natural thirst, which likely reflects day-to-day dynamics of InsCtx cue responses (Fig. 5G,H; Livneh et al., 2017). In addition, neurons' cue response *magnitudes* were correlated between natural thirst and SFO^{GLUT} activation ($r = 0.3$, $p = 5\times10^{-4}$). In summary, SFO^{GLUT} activation in a quenched state largely restores InsCtx water cue responses to a thirst-like state, similar to the restoration of food cue responses upon AgRP activation (Livneh et al., 2017). This led us to ask whether SFO^{GLUT} activation would also restore thirst-related patterns of *ongoing activity*, which reflect a dehydration state (Figs. 2–3).

We considered InsCtx ongoing activity during a two-day experiment. On Day 1, we imaged InsCtx during task engagement as mice gradually became quenched, as described above. We repeated this procedure on Day 2, but then injected CNO to activate SFO^{GLUT} neurons following the transition to the quenched state (same mice as in Fig. 5). As described in Fig. 3, we trained a classifier on thirsty vs. quenched epochs on Day 1 and tested it on all time points during Day 2. Surprisingly, we found that while SFO^{GLUT} activation restored cue responses (Fig. 5), it did *not* restore the pattern of InsCtx ongoing activity to a thirst-like pattern (Fig. 6A,B).

These findings prompted us to ask whether the same would hold true for AgRP activation. We reanalyzed data from our previously published experiments using a two-day protocol across states of hunger, satiety, and satiety + AgRP activation (Livneh et al., 2017). We trained the classifier on hungry vs. sated data from Day 1 and tested it on Day 2 data during satiety and AgRP activation (Fig. 6C,S5C). We found that while AgRP activation restored cue responses (Livneh et al., 2017), it did not restore ongoing activity to a hunger-like pattern (Fig. 6C). Therefore, our results suggest that InsCtx may maintain a faithful representation of a given physiological state, even upon activation of hypothalamic neurons that promote behavioral and InsCtx responses to need-relevant cues.

To further test this conclusion, we performed a loss-of-function experiment. Due to hierarchical organization of lamina terminalis thirst circuitry (Augustine et al., 2018a), we chose to inhibit its major output node – $MnPO^{GLUT}$ neurons. To do so, we chemogenetically inhibited MnPO Nos1+ glutamatergic neurons using hM4Di (Fig. 6D), which has been shown previously to robustly suppress thirst (Augustine et al., 2018a). Inhibition of $MnPO^{GLUT}$ neurons in thirsty mice using the chemogenetic ligand Compound 21 (C21), strongly suppressed behavioral responses to water cues (Fig. 6E, *Day 2*), while control saline injections did not (Fig. 6E, *Day 1*). InsCtx responses to learned water cues were also strongly suppressed (Fig. 6F). Importantly, C21 injection in the absence of hM4Di did not reduce task performance (Fig. S5D).

We then examined InsCtx ongoing activity in a two-day experiment. On Day 1, we imaged InsCtx during a brief recording in the thirsty state, followed by a control low volume saline injection. We then kept imaging across thirsty and quenched states, as described above. On Day 2, we performed a brief recording in the thirsty state, followed by injection of C21 to inhibit $MnPO^{GLUT}$ neurons. Finally, we rehydrated mice by systemic injection of isotonic

Author Manuscript Author Manuscript Author Manuscript Author Manuscript

saline (1 mL), which did not affect behavior but likely restored blood volume and, in part, blood osmolality. We trained the classifier on thirsty vs. quenched states on Day 1, and tested it on Day 2. Strikingly, InsCtx ongoing activity patterns on Day 2 were largely similar between periods when dehydrated mice were engaging in the task vs. when their task engagement was suppressed by $MnPO^{GLUT}$ inhibition (Fig. 6G). Importantly, however, subsequent rehydration via isotonic saline injection caused ongoing activity patterns in InsCtx to become more similar to those observed during a quenched state (Fig. 6G).

InsCtx Responses to Learned Cues and Consumption May Reflect a Prediction of Future Satiety

Theoretical models of human interoception suggest that InsCtx cue responses represent a prediction, or simulation, of a future interoceptive state (Barrett and Simmons, 2015; Owens et al., 2018; Quadt et al., 2018). Our data presented an opportunity to test this idea at cellular resolution across large populations of neurons in InsCtx of thirsty mice (Fig. 7), by comparing transient *cue-evoked* changes in neuronal population activity to the patterns of *ongoing activity* reflecting thirsty and quenched states. We hypothesized that presentation of a cue predicting water availability (and subsequent consumption of a drop of water) would rapidly modify the pattern of InsCtx activity to resemble the quenched pattern of ongoing activity within seconds, prior to absorption of water and changes in blood osmolarity (Fig. 7A).

During a thirsty state, neurons whose ongoing activity was higher in the quenched vs. thirsty state increased their activity within seconds of water cue presentation, while the converse was true for neurons whose ongoing activity was lower in the quenched vs. thirsty state (Fig. 7B,C). Thus, the water cue-evoked response reflected a shift in population activity pattern towards the quenched state. A similar shift occurred in 9/9 experiments from 7 mice ($r = 0.32 \pm 0.07$). Accordingly, presentation of water cues during thirst caused a transient decrease in the classification of InsCtx activity patterns as matching the thirsty state (Fig. S6A,B).

To more directly assess the relative similarity between the water cue-evoked patterns and the ongoing activity patterns associated with thirsty/quenched states, we projected cue-evoked population activity patterns onto the axis traversing thirsty and quenched ongoing activity patterns (Fig. 7A; Allen et al., 2019; Li et al., 2016), and scaled the resultant values between 1 (thirsty) and 0 (quenched). Water cues (but not other cues) and associated consumption during the thirsty state transiently shifted InsCtx activity patterns towards a quenched state (from values closer to 1 to values closer to 0) within seconds, despite the fact that water absorption occurs only minutes later and actual quenching occurs ~30–120 minutes later. This was true for individual mice (Fig. 7D, *left*), and when averaged across all mice (Fig. 7D, *right*). During gradual quenching across the session, ongoing activity patterns (prior to cue onset) gradually became more similar to those observed during the quenched state (Fig. 7E; similar to results obtained with a classifier, Fig. 3). Importantly, regardless of the current hydration state, water cues and associated consumption transiently shifted the pattern of activity, on average, to precisely the pattern associated with the future quenched state (Fig. 7E).

Author Manuscript Author Manuscript Author Manuscript Author Manuscript

These cue-evoked shifts were not simply due to the larger magnitude of neural responses to water cues vs. other cues (Fig. S6C), suggesting that they were caused by a change in the actual *pattern* of activity towards the quenched pattern. Furthermore, there were no systematic cue-evoked changes in population activity along a different axis linking activity patterns during high vs. low arousal (i.e., large vs. small pupil, approximately orthogonal to the thirsty vs. quenched axis; Fig. 7F).

During a quenched state, water cues did not affect InsCtx activity patterns (values near 0 in Fig. 7G, ***middle***). We then activated SFO^{GLUT} neurons during a quenched state. InsCtx ongoing activity patterns prior to cue presentation still reflected "quenched values" (~0), consistent with the classifier results (Fig. 6A,B). Remarkably, however, water cues shifted activity patterns further along the thirsty-quenched axis, *beyond* the quenched state to negative values (Fig. 7G, ***right***), suggesting a potential prediction of hypo-osmolarity and/or hyper-volemia (see Discussion).

Similar findings were also apparent in InsCtx during hunger and presentation of food cues. Specifically, in hungry mice, food cues and subsequent consumption transiently shifted ongoing activity patterns to the future sated state (Fig. 7H, ***right***). Further, food cues presented in the sated state did not shift the pattern of InsCtx activity (values remained ~0; Fig. 7H, ***middle***). However, under AgRP activation during a sated state, InsCtx activity began at "sated values" (~0) and food cue presentation and food consumption then shifted the activity further along the hungry-sated axis, beyond the sated state (Fig. 7H, ***right***). This may reflect a prediction of a physiological state associated with overconsumption.

Discussion

We combined two-photon calcium imaging with circuit mapping and manipulations to investigate InsCtx representations of physiological need states and need-relevant predictive cues. InsCtx neurons exhibited a thirst-dependent water cue response bias, similar to their hunger-dependent food cue bias (Livneh et al., 2017). Two-photon imaging of BLA axons in InsCtx further implicated BLA as an important source of learned cue information for InsCtx (Livneh et al., 2017; Samuelsen et al., 2012). Different patterns of *ongoing* activity in InsCtx were associated with specific physiological states (thirsty vs. quenched, hungry vs. sated) in a manner that did not merely reflect behavioral engagement or arousal. Artificial activation of hypothalamic hunger/thirst neurons restored responses to need-relevant cues in InsCtx, potentially by converging on a common PVT→BLA→InsCtx pathway. However, this artificial activation did not restore InsCtx ongoing activity to patterns reflecting physiological states associated with food/water deficit. Furthermore, artificial inhibition of hypothalamic thirst neurons reduced behavioral and InsCtx responses to water cues, while ongoing activity was largely unaffected. These results suggest that physiological state information reaches InsCtx via pathways that are not gated by hypothalamus (Fig. 8A). Importantly, during natural hunger/thirst, food/water cues transiently shifted InsCtx population activity towards patterns associated with future satiety states. During artificial hunger/thirst, these cues shifted the population activity beyond the satiety-related pattern. We propose that hypothalamic hunger/thirst neurons gate transmission of information

Author Manuscript Author Manuscript Author Manuscript Author Manuscript

regarding need-relevant cues to InsCtx, where these cue responses transform a representation of current physiological state to a transient prediction of a future physiological state.

Circuit Mechanisms Underlying InsCtx Responses to Predictive Cues

A large body of work in humans and animal models has established that InsCtx responds to learned cues predicting various salient outcomes (Becker et al., 2015; Fazeli and Buchel, 2018; Frank et al., 2013; Huerta et al., 2014; Kusumoto-Yoshida et al., 2015; Livneh et al., 2017; Naqvi et al., 2014). Recent work in rodent models has begun to reveal the circuit mechanisms that underlie hunger-dependent food cue responses in InsCtx (Kusumoto-Yoshida et al., 2015; Livneh et al., 2017). We now show that, as in humans (Becker et al., 2015), mouse InsCtx also exhibits thirst-dependent water cue responses, further supporting the generality of these findings (Fig. 1; Livneh et al., 2017).

Pharmacological and chemogenetic silencing experiments by our lab and others have pointed to the BLA as critical for behavioral and InsCtx neuronal responses to motivationally salient cues during hunger or thirst (Kim et al., 2016; Livneh et al., 2017; Namburi et al., 2015; Samuelsen et al., 2012). We directly imaged the activity of BLA axons in InsCtx, and observed both thirst- and hunger-dependent responses to water/food cues (Fig. 1, S1). Taken together, this evidence suggests that BLA plays an instructive role in the routing of salient cue information to InsCtx across different motivational states, including thirst and hunger.

We previously combined circuit mapping and manipulations to implicate a PVT→BLA pathway by which hunger, via hypothalamic AgRP “hunger neurons”, modulates InsCtx food cue responses (Livneh et al., 2017). Our current work suggests that thirst-promoting $MnPO^{GLUT}$ neurons and AgRP neurons converge onto common PVT→BLA neurons (Fig. 4). Intriguingly, PVT is also a site of convergence of other hypothalamic populations that promote distinct motivational drives, such as temperature regulation, aggression, and parental behavior (Hashikawa et al., 2017; Kohl et al., 2018; Tan et al., 2016). This convergence suggests that PVT may be a major hub that integrates information from multiple hypothalamic populations to modulate, and perhaps prioritize, cortical processing of need-relevant predictive cues (Fig. 8B; Hashikawa et al., 2017).

Physiological State Representations in InsCtx

Neuroimaging studies in humans have suggested that InsCtx ongoing activity reflects hunger and thirst (Egan et al., 2003; Meier et al., 2018; Tataranni et al., 1999). Further, an elegant recent study showed that InsCtx is the only cortical site whose activity tracks bodily physiology, and not “subjective water satiety”, while anterior cingulate cortex tracked subjective water satiety (Meier et al., 2018). These and other studies suggest that InsCtx integrates multiple types of sensory information to represent physiological hydration state (Augustine et al., 2018b; de Araujo et al., 2003; Gizowski and Bourque, 2018; Johnson and Thunhorst, 1997; McKinley et al., 2019; Zimmerman et al., 2017). However, the underlying neuronal population dynamics and circuitry remained unknown.

Using cellular-resolution population imaging, we showed that InsCtx ongoing activity patterns represent physiological need states (Fig. 2,3). These representations were consistent

Author Manuscript Author Manuscript Author Manuscript Author Manuscript

across days, independent of behavioral engagement, independent of arousal levels, and different for thirst and hunger. Most importantly, experiments involving artificial manipulation of hypothalamic hunger/thirst neurons allowed us to dissociate two aspects of InsCtx activity: ongoing activity patterns related to physiological state vs. cue/consumption-related activity related to food/water seeking and consumption (Fig. 5,6). Our findings suggest that InsCtx summates (Arieli et al., 1996) independent sources of input conveying information regarding either current physiological state (e.g., brainstem, visceral thalamus) and availability of food/water (BLA; Fig. 8B). Analogous results have been observed for InsCtx gustatory function, by dissociating cue- and taste-related InsCtx activity (Samuelsen et al., 2012, 2013). We speculate that BLA sends cue information to InsCtx, while InsCtx sends current and anticipated physiological state information back to BLA. This reciprocal loop might update the motivational salience and valence of predicted outcomes to inform decision-making (Klavir et al., 2013).

Recent studies in mice have found that fluctuations in behavioral state and arousal are major contributors to ongoing activity patterns throughout cortex, amygdala, and other subcortical structures (Allen et al., 2019; Grundemann et al., 2019; Musall et al., 2019; Salkoff et al., 2019; Stringer et al., 2019). Our InsCtx data likely contain information of this sort, particularly during periods of task disengagement (Fig. S3F,G). Our analytical approach and conclusions rely heavily on exclusion of any data from periods involving overt behaviors (e.g., licking or consumption), and on the reliability of ongoing activity patterns across days. This allowed us to identify representations of physiological state that are largely distinct from those of behavioral state/arousal, or from any within-day imaging artifacts (e.g., axial drift in imaging plane). Several lines of evidence support this conclusion. Our findings were not dependent on task engagement, differences in arousal level (as reflected by pupil dilation) or time-elapsed, and were not observed in other cortical areas. Additionally, activation of hypothalamic hunger/thirst neurons, which induced the same behaviors that occur during natural hunger/thirst, did not modify representations of physiological state in InsCtx ongoing activity. Moreover, while inhibition of hypothalamic thirst neurons reduced motivated behavior and left ongoing InsCtx activity largely unaffected, partial systemic rehydration produced a robust shift in the pattern of ongoing activity to that associated with the natural quenched state. Critically, during both thirst neuron inhibition and systemic rehydration, there was no overt behavior, and InsCtx ongoing activity could be shifted from a “thirsty” to a “quenched” state solely by a peripheral manipulation of hydration state.

A recent study used high-density electrophysiology throughout the brain across thirsty, quenched, and SFO^{GLUT} activation states (Allen et al., 2019). This study found that brain-wide representations of thirst state were largely restored upon SFO^{GLUT} activation. Such widespread restoration may reflect, at least in part, differences in arousal and in task engagement-related behaviors. The contributions of behavioral state/arousal to brain-wide changes in activity in this and other studies (Musall et al., 2019; Stringer et al., 2019) are distinct from the more restricted representations of physiological state that we observed in InsCtx. Our findings that SFO^{GLUT}/AgRP activation and $MnPO^{GLUT}$ inhibition do not affect thirst/hunger-like ongoing activity in InsCtx (Fig. 6) further support this conclusion. Interestingly, Allen et al. (2019) also observed a small subset of brain regions whose ongoing activity was not restored to a thirsty state by SFO^{GLUT} activation, such as prelimbic

Author Manuscript Author Manuscript Author Manuscript Author Manuscript

and retrosplenial cortices. We speculate that the information regarding physiological state in InsCtx may be relayed to prelimbic cortex to provide a specific interoceptive context in which cue-outcome associations are learned (Euston et al., 2012).

Interoceptive Predictions in InsCtx

Recent models propose that interoception involves not only sensing of current signals from the body, but also anticipation of future bodily signals (Barrett and Simmons, 2015; Owens et al., 2018; Paulus et al., 2019; Quadt et al., 2018). These predictive coding models suggest that InsCtx should contain distinct representations of current physiological state and predictions of future physiological state, which can then be combined to compute interoceptive prediction errors. Consistent with this model, we found InsCtx representations of current physiological state. Furthermore, predictive cues and subsequent consumption of a single drop of water/food in thirsty/hungry mice shifted InsCtx activity patterns to precisely the pattern observed in ongoing activity during the future sated state, regardless of the current level of food/water deficit (Fig. 7). These findings provide cellular-resolution evidence for the interoceptive prediction model of InsCtx function, and open up new opportunities for future investigations of interoceptive prediction errors.

Our findings support a heuristic framework for the roles of ongoing and learned cue-evoked activity in InsCtx. Specifically, each of multiple need states may be represented in InsCtx via a specific activity pattern, distinct from the activity pattern during a replete state (eucaloric, euhydrated, euthermic, etc.), along a distinct axis in the space of InsCtx population activity (Fig. 8C). This replete state activity may reflect a set point, and deviations in activity pattern along various axes (calories, hydration, temperature, etc.) may reflect competing homeostatic pressures. This is similar to recently proposed models (Juechems and Summerfield, 2019; Keramati and Gutkin, 2014) based on drive reduction theories of motivation (Hull, 1943). Furthermore, need-relevant predictive cues may transiently shift population activity along one or multiple axes (Fig. 7, 8C). Critically, readout of such population activity could allow estimates of both *specific* values along different axes, and the *overall* predicted value, of a given action. This framework can explain the contribution of InsCtx to decision-making.

This framework may also be relevant to understanding gustatory functions of InsCtx. For example, InsCtx represents taste palatability (Katz et al., 2001; Levitan et al., 2019b), which predicts absorption of calories and necessary nutrients (sugar, salt, protein). Thus, taste-evoked InsCtx activity could represent a prediction of the physiological consequences of consumption. In addition, InsCtx is necessary for conditioned avoidance of a taste associated with subsequent malaise, possibly by transforming a palatable taste cue representation to one that predicts physiological aspects of malaise (Accolla and Carleton, 2008; Grossman et al., 2008; Lavi et al., 2018).

Compromised interoception is considered an important element of different psychiatric conditions, including eating disorders, addiction, anxiety, and mood disorders (Khalsa et al., 2018). Therefore, establishing animal models that can complement studies in humans will be crucial for developing a mechanistic understanding of InsCtx dysfunction in these diverse psychiatric conditions. Our current and previous studies (Livneh et al., 2017) provide a

Author Manuscript Author Manuscript Author Manuscript Author Manuscript

framework for achieving this goal. First, we developed an approach for sub-cellular resolution imaging of InsCtx in awake, behaving mice. Second, we demonstrated that mouse InsCtx recapitulates key findings in humans, and then took advantage of mouse genetic tools to provide mechanistic insights into the underlying neural circuit mechanisms. We now also make initial steps to test theories of interoceptive predictive coding in humans. We speculate that modified InsCtx cue responses and associated behavioral consequences in patients with eating disorders might reflect a difference in the InsCtx representation of the hungry and/or sated state (i.e., the set point). More generally, this framework should allow examination of potential dysregulation of central representations of current and predicted interoceptive states in a range of diseases in psychiatry and medicine.

STAR Methods

LEAD CONTACT AND MATERIALS AVAILABILITY

This study did not generate new unique reagents. Further information and requests for resources and reagents should be directed to and will be fulfilled by the Lead Contact, Mark Andermann (manderma@bidmc.harvard.edu).

EXPERIMENTAL MODEL AND SUBJECT DETAILS

All animal care and experimental procedures were approved by the Beth Israel Deaconess Medical Center Institutional Animal Care and Use Committee. Animals were housed with standard mouse chow (Teklad F6 Rodent Diet 8664; 4.05 kcal g^{-1}, 3.3 kcal g^{-1} metabolizable energy, 12.5% kcal from fat; Harlan Teklad) and water provided *ad libitum*, unless specified otherwise. Mice used for *in vivo* two-photon imaging (age at surgery: 9–15 weeks) were instrumented with a headpost and a 2 mm microprism, centered over the mid InsCtx (see below and Livneh et al., 2017). All transgenic mice used in these studies were on the C57BL/6J background. We used male mice for *in vivo* imaging and for food/water intake studies. For CRACM experiments, we used both male and female mice and did not observe any differences between them. Portions of the data in Figures 6, 7, and S3 involve new analyses of previous datasets (Burgess et al., 2016; Livneh et al., 2017).

METHOD DETAILS

Sample sizes were chosen to reliably measure experimental parameters, while remaining in compliance with ethical guidelines for minimizing animal use and keeping with standards in the relevant fields. Different animals in each experimental group served as replicates, and multiple repetitions of each cue also served as within-mouse replicates. Experiments did not involve experimenter-blinding, but randomization was used with respect to trial order and data collection. Animal subjects were not randomly allocated to experimental groups as all comparisons were performed within subject.

Behavioral training—After at least 1 week of post-surgical recovery, animals (10–16 weeks old) were water restricted to ~80% of their free-feeding body weight or food-restricted to ~85% of their free-feeding body weight. Animals were head-fixed on a custom 3D printed wheel for habituation prior to any behavioral training (10 minutes to 1 hour over the course of 2–3 days). If the mice displayed any signs of stress, they were immediately

Author Manuscript Author Manuscript Author Manuscript Author Manuscript

removed and additional head-fixation sessions were added until there were no visible signs of stress. On the final head-fixation session, water-restricted and food-restricted animals were given water or Ensure (a high calorie liquid meal replacement) by hand via a syringe to acclimate them to licking water/Ensure. To train the animals to associate licking a lickspout with delivery of water/Ensure, we initially triggered delivery of water/Ensure (2–3 μL water, 5 μL Ensure - 0.0075 calories) to occur with every lick (with a minimum inter-trial interval of 2.5 s between Ensure deliveries). We tracked licking behavior via a capacitance-sensing lickspout (3D printed in a metal-containing filament connected to the MPR121 capacitance sensor). All behavioral training was performed using MonkeyLogic (Asaad and Eskandar, 2008).

Once water or food-restricted and head-fixed mice reliably licked to obtain a water/Ensure reward, we introduced the water/food cue (‘Go’ trials involving an initially arbitrary visual stimulus, see below for more details). We initially trained animals by presenting the water/food cue followed by unconditional delivery of the water/Ensure reward (Pavlovian reward). Once animals were regularly licking in response to the Pavlovian water/food cue but prior to reward delivery, we transitioned them to delivery of an operant reward, conditional on the animal licking during the response window (i.e. during the 2 sec post stimulus offset, see below for more details). After animals demonstrated stable licking behavior to the operant water/food cue (licking in response to >80% of trials involving food cue presentation), we simultaneously introduced ‘No-Go’ trials involving presentation of an operant aversive cue or of a neutral cue. Licking during the response window of the aversive cue resulted in the delivery of 2–3 μL of 1 M NaCl for water-restricted mice and 1 mM quinine for food-restricted mice. Licking to the neutral cue had no outcome. Initially, we biased the total number of trials towards the reward cue (reward cue : quinine cue : neutral cue, 2:1:1), but over several days we slowly increased the fraction of aversive and neutral cue trials so that all visual cues were presented in equal proportions. Animals typically learned to perform the visual discrimination task in ~2 weeks. We have previously shown that the InsCtx bias to the reward-predicting cue is independent of this training protocol (Livneh et al., 2017).

We began all imaging and behavior sessions with 2–5 Pavlovian reward cue trials, which served as “behavioral reminders.” Pavlovian reward cue trials also occurred sporadically during imaging (5–10% of trials). These trials were helpful in maintaining engagement, particularly during late stages of training. None of these Pavlovian reward cue presentations were included in the analysis of water/food cue responses.

The Go/NoGo task required water or food-restricted mice to discriminate between square-wave drifting gratings differing in orientation. The LCD screen (Dell) used to deliver visual stimuli was positioned ~20 cm from the mouse’s eye. All visual stimuli were presented as movies designed in Matlab (2 Hz and 0.04 cycles/degree, full-field square wave drifting gratings, 80% contrast; food cue: 0°, aversive cue: 270°, neutral cue: 135° (Burgess et al., 2016). All drifting gratings were presented for 2 sec, after which the mouse had a 2 sec window to respond with a lick. Licking during the visual cue was not punished, but also did not trigger delivery of the water/Ensure/salt-water/quinine. Only the first lick (if any) occurring during the response window triggered delivery of water/Ensure/salt-water/quinine. The lickspout was designed with two adjacent lick tubes (one for each outcome), such that

Author Manuscript Author Manuscript Author Manuscript Author Manuscript

the tongue contacted both tubes on each lick, which served as an effective deterrent for lick responses following aversive cues. Well-trained mice had a high rate of correct water/food cue licking responses (criterion: >80% of trials, usually ~90–95%), and a low rate of licking following aversive cue presentations (criterion: <50%, usually ~20–30%; Figure S1A,D).

Surgical procedures

Stereotaxic injections: Stereotaxic injections were performed as previously described (Livneh et al., 2017). Mice were anesthetized with isoflurane in 100% O_2 (induction, 3%; maintenance, 1–2%), and placed into a stereotaxic apparatus (Kopf model 963 or Stoelting). After exposing the skull via a small incision, a small hole was drilled for injection. A pulled-glass pipette with 20–40 μm tip diameter was inserted into the brain, and virus was injected using an air pressure system (Picospritzer). A micromanipulator (Grass Technologies, model S48 stimulator) was used to deliver the injection at 25 nl/min and the pipette was withdrawn 5 min after injection. For postoperative care, mice were injected intraperitoneally with meloxicam (0.5 mg/kg). Mice were 8–14 weeks old at the time of injection, except for CRACM experiments, for which mice were 7–10 weeks old.

We used the following volumes of virus and injection coordinates: InsCtx (100–200 nl, Bregma: AP: 0.0, 0.4 mm, DV: −4.1, −4.3 mm, ML: ~4.0 mm), SFO (50 nl per DV depth, Bregma: AP: −0.65 mm, DV: −2.3/−2.45/−2.6 mm, ML: 0 mm), MnPO (50 nl, Bregma: AP: +0.5 mm, DV: −5.2 mm, ML: 0 mm), ARC (200 nl, Bregma: AP: −1.45 mm, DV: −5.85 mm, ML: ±0.25 mm), PVT (25–50 nl, Bregma: AP: −1.0, −1.3 mm, DV: −3.0, −3.0 mm, ML: 0.0, 0.0 mm), BLA (100 nl, Bregma: AP: −1.6 mm, DV: −4.5, −4.76 mm, ML: ±3.3 mm).

Optic fiber implantation for optogenetic stimulation: First, mice were stereotaxically injected with AAV1-DIO-ChR2(H134R)-YFP into the MnPO, as described above. An optic fiber (200-μm diameter core; BFH37–400 Multimode; NA 0.52; Thor Labs) was then implanted over the PVT (AP: −1.3 mm, DV: −2.8 mm, ML: 0.0 mm from Bregma). The fiber was fixed to the skull using C&B Metabond (Parkell). Mice were allowed at least 3 weeks for recovery before behavioral testing started.

Microprism assembly and surgery: Glass microprism assemblies were fabricated using standard 2 mm prisms (#MCPH-1.0; Tower Optical) coated with aluminum along their hypotenuse. Prisms were attached to a coverglass (#1 thickness), both along the hypotenuse (to prevent scratching of the reflective surface) and at the side of the prism that faces InsCtx, using Norland Optical Adhesive 71 cured using ultraviolet light.

Approximately 1–2 weeks following AAV-GCaMP6f injection into InsCtx, mice (10–16 weeks old) were anesthetized using isoflurane in 100% O_2 (induction, 3%; maintenance, 1–1.5%) and placed into a stereotaxic apparatus (Kopf) above a heating pad (CWE). Ophthalmic ointment (Vetropolycin) was applied to the eyes. Using aseptic technique, a custom-made headpost was secured using cyanoacrylate glue, dental acrylic and C&B Metabond (Parkell). A 2.2×2.2 mm^2 craniotomy was then performed over the left InsCtx and S2 (bottom edge of the craniotomy was just above the squamosal plate), centered around the AP location of the previously performed AAV-GCaMP6f injections. A 2×2 mm^2 microprism

Author Manuscript Author Manuscript Author Manuscript Author Manuscript

was then stereotaxically lowered into the craniotomy until contact with the InsCtx was made, and was then lowered further with concomitant movement medially (~100–200 μm) until contacting the top edge of the craniotomy, while verifying that the microprism's bottom edge was inserted below the squamosal plate. Once the prism was in place, the window edges were affixed to the skull using Vetbond (3M), followed by C&B Metabond (Parkell) to form a permanent seal. A 1:3 dental cement mix of black powder paint (Black) and white dental acrylic (Dentsply) was then applied for light shielding. Meloxicam (0.5 mg per kg, s.c.) was administered and the mouse was allowed to recover. We imaged and included in analyses all animals with implanted microprisms and adequate microprism clarity for imaging.

Two-photon imaging across different natural and artificial states—Two-photon imaging was performed using a resonant-scanning two-photon microscope with tiltable scanhead (Neurolabware; 31 frames/second; 1154×512 pixels). All imaging was performed with a 20×0.45 NA air objective (Olympus) with a 540 × 360 μm^2 field of view. All imaged fields of view (FOV) were at a depth of 90–200 μm below the pial surface, using a Mai Tai DeepSee laser (Newport Corp.) with laser power at 920–960 nm of 35–80 mW at the front aperture of the objective (power at the sample was likely substantially less due to partial transmission via the microprism). Imaging depth was adjusted in between runs (every 30 min) to account for slow drift in the z plane (< 7 μm).

Imaging across thirsty/quenched and hungry/sated states: To assay how changes in thirst/hunger state affect behavior and neural activity, we imaged mice during either gradual or rapid satiation. In the *gradual satiation* condition (only for water-restricted mice), we imaged mice during consecutive 30-minute runs until the mice voluntarily stopped performing the task. We then performed one more imaging run, the 'quenched' run, in which mice did not respond to the water cue. We never observed re-engagement of the mice in the task during the quenched run, in contrast to re-feeding in food-restricted mice (Livneh et al., 2017).

In the *rapid satiation* condition, we imaged mice in two blocks of trials within a session, one block during water/food restriction and a subsequent block immediately following re-hydration/re-feeding. At the start of each imaging session, water/food-restricted mice (~80% or ~85% of free-feeding weight, respectively) performed the visual cue discrimination task. After ~180 trials (30-min imaging run), we provided the mouse with *ad libitum* access to water or Ensure until voluntary cessation of consumption. Water consumption lasted 2–5 minutes, while Ensure consumption lasted 45–75 minutes, using the same protocol for acclimating mice to the lick-spout (see above). During this period of time, mice consumed ~1 mL of water (in task involving water restriction) or ~3–5 mL of Ensure (in task involving food restriction) and then voluntarily stopped licking for rewards. We then imaged additional ~180 trials (30 min imaging run) while mice were quenched/sated (operationally defined as the absence of voluntary licking). Importantly, we have previously shown that InsCtx biased cue responses track motivational salience and are not observed in naïve mice (Livneh et al., 2017).

Author Manuscript Author Manuscript Author Manuscript Author Manuscript

Imaging during chemogenetic activation of SFO^{GLUT} neurons: We initially screened mice for successful targeting of AAV8-CaMKII-hM3Dq-mCherry to SFO by measuring CNO-induced drinking behavior (see details in 'Water intake and food intake studies' section below). If mice displayed significant drinking, they underwent further AAV-GCaMP6 injections and microprism implant surgeries, followed by behavioral training (see above). We then imaged mice across thirsty and quenched states, as described above. We verified post-mortem that mice that did not drink following CNO injection also did not express hM3Dq-mCherry in the SFO. We usually did not detect hM3Dq-mCherry anywhere in the brains of these mice, and therefore conclude that the injections were likely mis-targeted to the ventricle. Importantly, as CNO did not induce drinking in these mice, they demonstrate that CNO itself is not sufficient to induce thirst in the absence of hM3Dq-mCherry expression (Figure S5A).

Following imaging during the quenched state, we injected 150 μl 0.9% saline on Day 1, or CNO (5 mg/kg) on Day 2, waited 10–15 min and started another imaging run (~180 trials, 30 min). For every mouse used for these experiments, we used postmortem histology and immunohistochemistry (see below) to verify hM3Dq-mCherry expression in the SFO.

The effects of CNO injections were not due to the actual pain caused by the injection. First, we verified that saline injections did not restore behavioral responses or neuronal responses in the same mice on the previous day (Figure S5B). Second, all mice were habituated with several saline injections before performing the actual CNO injections. Third, it is highly unlikely that a painful stimulus, such as an intraperitoneal injection, would cause food cue-biased responses in InsCtx. It remains possible that this would cause a general long-lasting increase in arousal. However, as our pupil-tracking data demonstrate, this should result in a *non-specific* increase in responses to all 3 cues (Figure S1). Therefore, because CNO injections restored water cue-biased responses (Fig. 5) and InsCtx cue bias tracks motivational salience (Livneh et al., 2017), it is highly unlikely this can be explained by the actual needle injection, rather than by activation of SFO^{GLUT} neurons.

Imaging during chemogenetic inhibition of MnPO^{GLUT} neurons: We initially "screened mice for successful targeting of AAV8-hSyn-DIO-hM4Di-mCherry to MnPO by measuring drinking behavior with 125 μl 0.9% saline vs. Compound 21 (C21) injections (see details in 'Water intake and food intake studies' section below). If mice displayed significant consistent inhibition of drinking, they underwent further AAV-GCaMP6 injections in InsCtx and microprism implant surgeries, followed by behavioral training (see above). Importantly, C21 did not affect behavior in the visual discrimination task in mice not expressing hM4Di (Fig. S5D). The effects of C21 injections were not due to the actual pain caused by the injection, as control saline injections on Day 1 did not affect behavior (Fig. 6E). For every mouse used for these experiments, we used postmortem histology and immunohistochemistry (see below) to verify hM4Di-mCherry expression in the MnPO.

Consecutive days in states of thirst and then hunger (Figure S3I): We initially trained mice during water-restriction on the water-seeking task. We then imaged mice while performing the task as usual on the first two days until they gradually reached a quenched state. After the second day's imaging session ended, we returned mice to their home-cage

Author Manuscript Author Manuscript Author Manuscript Author Manuscript

overnight with free access to food, but no access to water. On the third day, the visual stimulus predicting water now predicted liquid food. Mice required some initial retraining at the beginning of Day 3. We used two different protocols. In protocol #1, the fluid reward was water and the food reward was Ensure. In protocol #2, the fluid reward was (calorie-free) 1 mM sucralose solution and the food reward was (calorie-containing) 600 mM sucrose, roughly matching the sweetness of 1 mM sucralose, and the caloric content of Ensure (Domingos et al., 2011).

Pupil videography during two-photon imaging—We acquired data using a GigE Vision camera (Dalsa) with a 60 mm lens (Nikon MicroNikkor) from a pre-selected region of interest around the eye ipsilateral to the LCD monitor used to present visual cues (contralateral to the InsCtx microprism). Acquisition of each frame (frame rate of 15.5 Hz) was triggered on every other frame of two-photon acquisition (acquired at 31 Hz) using Scanbox software (Neurolabware). The pupil was backlit with illumination originating from diffusion within the brain of the IR light used for two-photon excitation during imaging. See below for details of data analysis.

Postmortem identification of imaging field location—We performed this procedure as previously reported (Livneh et al., 2017). We terminally anesthetized mice with an overdose of chloral hydrate (Sigma Aldrich), and then left them in their homecage for several hours to reduce subsequent blood loss during decapitation. We then decapitated mice, and postfixed their heads in 10% neutral buffered formalin (Fisher Scientific) overnight. We carefully removed and washed the brains. We then performed whole-mount imaging of the entire brain using light and fluorescence microscopy for visualization of surface vasculature and GCaMP6f fluorescence. Microprism location was evident by a minor indentation of the tissue. We then aligned the postmortem surface vasculature to *in vivo* epifluorescence images (imaged through the microprism) for coarse localization of the imaging field. For a more precise localization of the imaging field of view, we further aligned the vasculature to vascular landmarks from *in vivo* two-photon imaging. Finally, we used this information to localize imaging fields of view, relative to the middle cerebral artery and rhinal vein. We verified that our imaging field location matched the locations in our previous study (Livneh et al., 2017).

Brain tissue preparation and immunohistochemistry—Mice were terminally anesthetized with chloral hydrate (Sigma Aldrich) and transcardially perfused with phosphate-buffered saline (PBS) followed by 10% neutral buffered formalin (Fisher Scientific). Brains were extracted, cryoprotected in 20% sucrose, and sectioned coronally on a freezing sliding microtome (Leica Biosystems) at 30–40 μm, and collected in 3–4 equal series.

Brain sections were washed in 0.1 M phosphate-buffered saline pH 7.4, blocked in 3% normal donkey serum/0.25% Triton X-100 in PBS for 1 hour at room temperature and then incubated overnight at room temperature in blocking solution containing primary antiserum. The next morning, sections were extensively washed in PBS and then incubated in Alexa fluorophore-conjugated secondary antibody (Molecular Probes, 1:1000) for 2 h at room

Author Manuscript Author Manuscript Author Manuscript Author Manuscript

temperature. After several washes in PBS, sections were mounted onto gelatin-coated slides and fluorescent images were captured with an Olympus VS120 slide scanner microscope.

All antibodies used were previously verified. For all experiments that involved stereotaxic injections (e.g., anatomical tracing, *ex vivo* CRACM, optogenetic and chemogenetic behavioral and imaging studies), we verified infection in the desired brain region with minimal spillover outside it, and excluded animals with imprecise injections.

Rabies collateral mapping—Similar to previously described procedures (Betley et al., 2013; Livneh et al., 2017), three weeks after unilateral injection of AAV8-EFIα-DIO-TVA-mCherry into the MnPO/OVLT (in vGLUT2-ires-Cre mice), SADΔG–EGFP (EnvA) rabies was injected into the PVT (for coordinates, see above). Animals were allowed 5 days for retrograde transport of rabies virus and EGFP transgene expression in long-range axons before perfusion, tissue collection and imaging (Olympus VS120 slide scanner microscope). The GFP signal was amplified using immunohistochemistry to visualize weakly labeled axons.

Slice electrophysiology and channelrhodopsin-assisted circuit mapping (CRACM)—For brain slice preparation, mice 8–12 weeks old were anesthetized with isoflurane before decapitation and removal of the entire brain. Brains were immediately submerged in ice-cold, carbogen-saturated (95% O_2, 5% CO_2) choline-based cutting solution consisting of (in mM): 92 choline chloride, 10 HEPES, 2.5 KCl, 1.25 NaH_2PO_4, 30 $NaHCO_3$, 25 glucose, 10 $MgSO_4$, 0.5 $CaCl_2$, 2 thiourea, 5 sodium ascorbate, 3 sodium pyruvate, oxygenated with 95% O_2/5% CO_2, measured osmolarity 310 – 320 mOsm/L, pH= 7.4. Then, 300-μm-thick coronal sections were cut with a vibratome (Campden 7000smz-2) and incubated in oxygenated cutting solution at 34°C for 10 min. Next, slices were transferred to oxygenated aCSF (126 mM NaCl, 21.4 mM $NaHCO_3$, 2.5 mM KCl, 1.2 mM NaH_2PO_4, 1.2 mM $MgCl_2$, 2.4 mM $CaCl_2$, 10 mM glucose) at 34°C for 15 min and then stored in the same solution at room temperature (20–24°C) for at least 60 min prior to recording. A single slice was placed in the recording chamber where it was continuously superfused at a rate of 3–4 mL per min with oxygenated aCSF. Neurons were visualized with an upright microscope equipped with infrared-differential interference contrast and fluorescence optics. Borosilicate glass microelectrodes (5–7 MΩ) were filled with internal solution.

For CRACM of inputs from $MnPO^{GLUT}$ neurons onto PVT→BLA neurons, light-evoked EPSCs were recorded in whole-cell voltage-clamp mode, with membrane potential clamped at −70 mV using a using a Cs^+-based low Cl^- internal solution consisting of (in mM): 135 $CsMeSO_3$, 10 HEPES, 1 EGTA, 4 $MgCl_2$, 4 Na_2-ATP, 0.4 Na_2-GTP, 10 Na_2-phosphocreatine (pH 7.3 adjusted with CsOH; 295 mOsm · kg^{-1}; ECl = −70 mV). All recordings were performed using a Multiclamp 700B amplifier, and data were filtered at 2 kHz and digitized at 20 kHz. To photostimulate channelrhodopsin2-positive fibers, a laser or LED light source (473 nm; Opto Engine; Thorlabs) was used. The blue light was focused onto the back aperture of the microscope objective, producing wide-field illumination of the recorded cell at 10 mW/mm^2. The light power at the specimen was measured using an optical power meter PM100D (Thorlabs). The light output was controlled by a

Author Manuscript Author Manuscript Author Manuscript Author Manuscript

programmable Master-8 pulse stimulator (A.M.P.I.), and pClamp 10.2 software (Axon Instruments). The photostimulation-evoked EPSC detection protocol consisted of four blue light laser pulses administered 1 sec apart during the first 4 sec of an 8-sec sweep, repeated for a total of 30 sweeps. We attempted to maximize our ability to detect light-evoked currents by biasing our recordings to cell bodies within the densest axon fields. In some experiments, TTX (1 μM) and 4-AP (100 μM) was added to the bath solution in order to confirm monosynaptic connectivity. All CRACM results presented are from 2–3 mice per group.

Water intake and food intake studies—We assessed drinking using Drinking Event Monitor cages (lickometer cages; Columbus Instruments). We put individual male mice into lickometer cages where licks on each bottle sipper tube were detected by electrical conductivity and recorded by a computer counter interface (Resch et al., 2017). Initially, for training and acclimation, we water-deprived mice overnight. The next day, we placed mice into lickometer cages with free access to a water bottle for 30 min. We considered training sessions successful if mice accumulated ≥200 licks during the test. If not, we repeated them the following day. For subsequent SFO^{GLUT} chemogenetic activation and $MnPO^{GLUT}$→PVT optogenetic activation experiments, we let mice have *ad libitum* access to food and water for 1–2 days and then tested evoked drinking.

For SFO^{GLUT} chemogenetic activation, we measured drinking during two consecutive 30-minute sessions. The first session was a control session 10 minutes following saline injection, and the second session was 10 minutes following CNO injection (5 mg/kg).

For $MnPO^{GLUT}$ chemogenetic inhibition, we water-restricted mice for 24 hrs, and measured drinking during a 30-minute session, preceded by saline or C21 injection (5 mg/kg). Saline and C21 sessions were separated by two days and repeated 2–3 times per mouse, to verify the reliability of the effect.

For $MnPO^{GLUT}$→PVT optogenetic activation, we firmly attached fiber optic cables (1.0 m length, 200 μm diameter; Doric Lenses) to fiber optic ferrules with zirconia sleeves (Doric Lenses). Light pulse trains (7–10 mW, 10 ms pulses of 20 Hz; 1 sec on, 3 sec off) were programmed using a waveform generator (National Instruments) that provided TTL input to a blue light LED (465 nm; Plexon). We measured drinking during two consecutive 30-minute sessions. The first session was a control “light-off” session, and the second was the “light-on” session. Optogenetic stimulation began 1 min prior to access to water. Blue light stimulation in mice with mis-targeted injections did not induce drinking.

We used the same mice for water and food intake studies. For food intake studies during $MnPO^{GLUT}$→PVT optogenetic activation, we food-restricted mice overnight, and then measured the quantity of home-cage consumption during a two-hour period involving free access to chow. We measured feeding in “light-off” and “light-on” conditions on separate days, at least 4 days apart. For all water/food intake studies, we excluded from further analysis mice that demonstrated mis-targeted injections, fiber implants, or expression extending outside the area of interest, based on post-hoc histological examination,.

Author Manuscript Author Manuscript Author Manuscript Author Manuscript

QUANTIFICATION AND STATISTICAL ANALYSIS

Statistical tests were performed using standard Matlab (MathWorks) functions. Differences across mice (e.g., behavior) were tested using the t-test due to relatively small sample sizes. Differences in neural activity across large neural populations were tested using non-parametric tests (Kruskal-Wallis and Mann-Whitney tests) due to the non-normal distribution of the data. We did not assume equal/unequal variance in parametric t-tests as all t-tests were paired. All data analyses were performed using custom scripts in Matlab (MathWorks) or ImageJ (NIH).

Image registration and timecourse extraction—First, each acquired image was spatially downsampled by 2X. To correct for motion along the imaged plane (x-y motion), each frame was registered to an average field-of-view using efficient subpixel registration methods (Bonin et al., 2011). Within each imaging session, each run (2–8 runs/session) was registered to the first run of the day. Image stacks were de-noised using principal components analyses (PCA) of every pixel across time, and by user identification and removal of noise principal components (low eigenvalues; based on Mukamel et al., 2009). Cell/axon masks and calcium activity timecourses ('F(t)') were extracted using custom implementation of common methods (Mukamel et al., 2009). To avoid use of cell/axon masks with overlapping pixels, we only included the top 75% of pixel weights for a given mask (Ziv et al., 2013), but users screened each prospective ROI and could edit the size of the mask, selectively removing the lowest probability pixels. We then excluded any remaining pixels identified in multiple cell/axon masks. We manually verified that all cell masks had typical cell body morphology and size. In order to not count an axon multiple times, each BLA→InsCtx axon ROI included signal from all boutons and the axon shaft (Burgess et al., 2016; Mukamel et al., 2009). Additionally, to ensure we were not erroneously counting one BLA→InsCtx axon multiple times, we calculated the pairwise correlation coefficient of all simultaneously recorded BLA→InsCtx axon timecourses (all time-points, excluding 8 sec epochs starting at water/food cue onset. These include the cues, licking and water/Ensure reward, which could drive strong correlations) and combined the ROI masks for those with values higher than 0.6 (confirmed manually).

Fluorescence timecourses were extracted by averaging the pixels within each region-of-interest ('ROI') mask. Fluorescence timecourses for neuropil within a 25 μm annulus surrounding each ROI (but excluding adjacent ROIs and a protected ring surrounding each ROI) were also extracted ($F_{neuropil}(t)$: median value from the neuropil ring on each frame). Fluorescence timecourses were calculated as $F_{neuropil\_corrected}(t) = F_{ROI}(t) - F_{neuropil}(t)$. The change in fluorescence was calculated by subtracting a running estimate of baseline fluorescence ($F_0(t)$) from $F_{neuropil\_corrected}(t)$, then dividing by $F_0(t)$: $\Delta F/F(t) = (F_{neuropil\_corrected}(t) - F_0(t))/F_0(t)$. $F_0(t)$ was estimated as the 10th percentile of a 32 sec sliding window (Burgess et al., 2016; Livneh et al., 2017). All example cue-evoked timecourses were re-zeroed in the 1 sec prior to visual stimulus onset for visualization purposes only.

Alignment of cell masks across runs and across days—We chose one set of cell masks for each day. All analyses for the alignment of cell masks across days were semi-

Author Manuscript Author Manuscript Author Manuscript Author Manuscript

automated with the aid of a custom Matlab GUI. To align masks across two days, we first aligned the mean image from each day using one of three methods (depending on the degree of across-day image warping): a rigid body translation, an affine image translation (which allowed for across-day image rotation), or a Delauney triangulation image transformation (for more complex image warping). The alignment transformation used to register the mean image from each day was then applied to each individual mask. For each pair of overlapping ROIs, we calculated the 2D correlation of the PCA/ICA masks. Any ROIs with correlation values below 0.05 were ignored, as were any correlations lower than 0.5 below the value of the maximum correlation. The remainder of PCA/ICA masks were shown to the user, along with an average image of the peak 200 frames of the activity of that ROI. We kept only those ROIs with high correlations in which we could identify similar shapes of soma and processes in the maximum image on both days. Note that the image registration and warping techniques were applied to masks only for alignment suggestion purposes, and were never applied to cell masks for fluorescence timecourse estimation.

Single-neuron response analyses—We categorized cells as responsive to visual cues and/or licking and/or water/Ensure delivery. To determine if cells were responsive to *visual cues*, we independently tested the cue-evoked response of each cell to each type of cue for each day the cell was identified. For each cell, we compared activity in the 1 sec prior to stimulus onset to activity in a 200-ms sliding window beginning at stimulus onset and continuing until 100 ms before licking onset. This helped minimize contamination of estimates of early, visual cue-evoked responses with activity linked to licking behavior. Given the variability of licking onset across trials, we only analyzed time-points that preceded lick onset by >100 ms in at least 10 trials. The comparison of this post-stimulus activity with pre-stimulus baseline was performed using the Wilcoxon Signed-Rank test, followed by an FDR correction for multiple comparisons ($p<0.05$). All data were analyzed using time-points up to 100 ms before licking onset. However, we also separately repeated this analysis using data up to 200 ms or 300 ms before licking onset, and observed similar results (Livneh et al., 2017).

As previously shown, InsCtx neurons can exhibit responses that are temporally locked to licking in the absence of any prior sensory cues, and can begin either just before or just after lick-bout onset. The same is true for gustatory responses to liquid tastants, such as those to water and Ensure (see e.g., Katz et al., 2001; Levitan et al., 2019a; Samuelsen et al., 2012; Stapleton et al., 2006). Licking or water/Ensure responses can occur either just before (e.g., anticipatory) or just after licking or water/Ensure onset (i.e., somatosensory/gustatory). As such, to determine if cells were responsive to *licking* onset, we first aligned each trial to licking onset and tested whether activity changed significantly either just before (e.g., anticipatory) or just after licking onset. To assess responses that preceded licking, we performed the same procedure described above, but now comparing data during the one-second period prior to cue onset to the pre-licking period following cue onset. Additionally, to assess responses that occurred just after licking onset, we compared the 1 sec period prior to licking onset to the period from licking onset until 100 ms before Ensure delivery. We followed a similar procedure for calculating responses to *water/Ensure delivery*. We first aligned each trial to the time of water/Ensure delivery. Then, to assess responses that

Author Manuscript Author Manuscript Author Manuscript Author Manuscript

preceded water/Ensure delivery, we performed the same procedure described above, but now comparing data in the 1 sec prior to licking onset with data in the period prior to water/Ensure delivery. Additionally, to assess responses that occurred just after water/Ensure delivery, we compared the one-second period prior to water/Ensure delivery to the 4-sec period following water/Ensure delivery. After these initial analyses, cells/axons were categorized as responsive to licking if they were responsive to licking in either the pre-licking or post-licking periods (or both), and categorized as responsive to water/Ensure if they responded in either the pre-water/Ensure or post-water/Ensure periods (or both).

We ultimately sought to coarsely categorize cells/axons as responsive to visual cues and/or licking and/or water/Ensure delivery. As described above, cells were initially *independently* classified as responsive to visual cues, licking and/or water/Ensure. However, cells/axons may have responses that start at one epoch (e.g., excited by licking) and continue well into the following epoch (e.g., excited by water/Ensure). In such cases, we would consider the cell/axon only responsive to the initial epoch, unless the response changed in sign in the second epoch (e.g., excited by licking and then suppressed by Ensure). Thus, if a cell/axon was significantly responsive in more than one epoch (visual cue, licking, water/Ensure), in order for it to be categorized as licking or water/Ensure responsive, its response to either epoch had to be of opposite sign (excited/suppressed) as compared to the previous epoch, for cells in which the previous epoch also evoked a significant response.

We also assessed response magnitude of the average cue-evoked response. For each neuron, we used the maximal absolute value of the average cue response during the time of presentation of the two-second cue as its response magnitude.

Pupil diameter and its effects on cue-evoked responses (Figure S1C,F)—We measured pupil diameter from videography of the eye. For the first frame of the movie, we manually drew a region around the eye and marked the center of the pupil. The center and area of the pupil was then fit using a custom implementation of the starburst pupil detection from openEyes toolkit and a ransac algorithm. The center position from each previous frame was used to initialize the subsequent frame.

For analyses of the relationship between InsCtx activity and pupil diameter, we used our previously established procedure (Livneh et al., 2017). We first up-sampled the pupil diameter timecourse (from 15.5 Hz to 31 Hz) using linear interpolation. We then calculated the average pre-cue pupil diameter using the average of 1 sec before the presentation of each cue during hungry/thirsty and sated/quenched states. We then matched pre-cue pupil diameter using the following procedure. For every cue presentation (trial) during a hungry/thirsty state, we searched for a matching trial during a sated/quenched state from the same session. We first searched for all ‘sated/quenched trials’ that were within ±10% of the ‘hungry/thirsty trial’. Of these, we then selected the ‘sated/quenched trial’ that had the value nearest to the ‘hungry/thirsty trial’. Each trial from both states could only be analyzed once. Using this procedure, we could match ~50% of trials from both states (because pupil diameter was typically slightly smaller, on average, during sated/quenched states, usually the ‘sated/quenched trials’ with higher pupil diameter values were matched to a given ‘hungry/thirsty trial’). We then analyzed InsCtx data either from all trials or only from trials matched

Author Manuscript Author Manuscript Author Manuscript Author Manuscript

for pre-cue pupil diameter (such that the distribution of pupil diameters across all trials used was similar between hungry/thirsty and sated/quenched states).

Comparisons across natural and artificial thirst states for individual neurons (Figures 1,5)—We first aligned data from the two days of the experiment and only used neurons that were active on both days and could be reliably identified on both days. To facilitate comparisons of responses across states within an imaging day, and across states between days, we normalized the responses of each neuron within day across states, using a single transformation that was applied to all cue responses from a given neuron within the same-day session. We accomplished this by z-scoring each neuron's responses to the 3 visual cues across the two states within each day (i.e., z-scores from one distribution consisting of all cue presentations of all cue types during 'Thirsty', 'Quenched', and 'Quenched+SFO^{GLUT} activation'). Z-scoring was performed by $(x_i - \bar{x})/S$, where x_i is the ΔF/F value at time-point i, $\bar{x}$ is the average ΔF/F of all visual cue responses from that day (all timepoints from 1 sec before cue onset up to 100 ms before the first lick per trial or 2 sec post-cue onset in the case of trials in which no licking occurred during stimulus presentation; the average was across all trials, all visual cues, and all states), and S is the standard deviation of ΔF/F from all visual cue presentations from that day (all timepoints from −1 sec to ~2 sec relative to cue onset (up to 100 ms before first lick), across all trials, all visual cues, and all states). To capture changes from baseline, responses were re-zeroed such that pre-cue period mean was zero.

The 'hunger/thirst modulation index' was calculated for each neuron as $(R_{hungry/thirsty} - R_{sated/quenched})/(R_{hungry/thirsty} + R_{sated/quenched})$, where R is a neuron's average response during the entire visual cue (using timepoints up to 100 ms before the first lick in each trial, and for which such lick-free data existed for ≥10 trials). We assessed similarity across days by using a three-step approach. First, we calculated a 'state modulation index' (SMI) that was identical to the hunger/thirst modulation index, but that was used to compare any two states, either within or across days (e.g., two consecutive thirsty sessions, or thirsty vs. quenched). Second, to compare across-state similarity to inherent variability of responses over time in individual neurons, we also compared the similarity within state. We did this by assessing each neuron's reliability (or 'self-similarity') by randomly splitting up trials within a session and state into two halves and calculating the SMI between the two halves, and then repeating this analysis 100 times, to obtain a distribution of self-similarity. Third, we compared the actual SMI across states/days to the neuron's 'self-similarity' and classified it as similar if (i) both SMIs were between the 10th and 90th percentiles of the 'self-similarity' distribution and (ii) both SMIs had the same sign (excitation/suppression).

Generalized linear model of single neuron activity—To classify cell responses, we fit a Gaussian GLM to the activity of each cell (ΔF/F), accounting for task and behavioral variables (Driscoll et al., 2017; Friedman et al., 2010) using the glmnet package. We first downsampled the data by a factor of 2 and convolved the results with a Gaussian kernel of width 4 frames. We created a series of basis functions to describe task events and behavioral variables. These basis functions were a series of Gaussian curves separated by 4 frames, and with a full-width at half maximum of 4 frames. The basis functions spanned different time

Author Manuscript Author Manuscript Author Manuscript Author Manuscript

ranges surrounding each variable. We included the basis functions representing each cue type (food/water cue, neutral cue, and aversive cue), separated by trial type (hit, miss, correct reject, false alarm), and tiled across and beyond the entire cue duration (0–4 sec). We also included basis functions representing times relative to (i) any stimulus offset (0 to 4 sec surrounding offset), (ii) the presentation of reward outcome or aversive outcome (−1 to 8 sec), (iii) the onset of a lick bout (−1 to 2 sec from bout onset, with lick bouts separated by ≥ 2 sec), (iv) all other individual licks (one kernel at the time of each lick), (v) brain motion (the kernel convolved with the analog vector) and (vi) locomotion (the kernel convolved with the running speed) or pupil diameter (the kernel convolved with the analog vector). The GLM was fit on two thirds of the data for each cell with elastic net regularization ($\alpha = 0.01$). We then used the GLM coefficients to measure the deviance explained on the remaining one third of the data (Figure 2B,C).

Estimation of InsCtx ongoing activity—We sought to minimize the effects of task-related activity on estimations of ongoing activity. To do so we used neuropil-subtracted fluorescence timecourses (not yet normalized to baseline fluorescence), and identified times that would be minimally affected by task performance – the last 3 sec of inter-trial intervals (ITIs, 6–8 sec), preceded by correct rejection trials (no licking) of the aversive cue, neutral cue and blank trials. Notably, as a result, the previous rewarded trial was 13–25 sec before the selected ITI period. Additionally, we removed any ITI epochs that had any licking. We then calculated the fractional change in activity (ΔF/F) of the concatenated fluorescence time series of this subset of ITI periods using the sliding window method, described above. This approach allowed us to estimate ongoing activity levels that are minimally affected by task performance and by task-independent licking.

Classification of ongoing activity—We used an extension to the Naïve Bayes classifier called an Averaged One-Dependence Estimator (AODE), which accounts for pairwise probabilities (Sugden et al., 2018; Webb et al., 2005) and does not make the false assumption that the activity of each neuron in a field of view is independent. The primary advantages of such a probabilistic classifier (i.e., one that uses Bayes' rule) are that all assumptions are made explicit and the values determined by the classifier are simple probabilities. The equation for the AODE is below, where y is the class (e.g., thirsty/quenched), x_i and x_j are the activity

$$P(y|x_1,\ldots,x_n) = \frac{\pi_y \sum_i P(x_i|y) \prod_{j\neq i} P(x_j|y,x_i)}{\sum_{y'} \pi_{y'} \sum_i P(x_i|y') \prod_{j\neq i} P(x_j|y',x_i)}$$

levels of two cells, and πy is the prior of class y.

We estimated the probability of a cell being active given a certain state by using the mean and standard deviation of its activity (ΔF/F) in that state. We estimated the probability of a pair of cells being co-active given a certain state by using the Pearson correlation coefficient. For classification using Naïve Bayes, we used the same estimations and formula, but without the terms involving pairwise probabilities of co-activity per state.

Author Manuscript Author Manuscript Author Manuscript Author Manuscript

To facilitate comparisons across days, prior to classification, each neuron's timecourse was z-scored per day. We then binned data into 1 sec bins for classification. The classifier was trained on two classes (e.g., thirsty vs. quenched), matching the number of observations per class. For within-day classification of these two classes, we used cross-validation (training on randomly selected 80% and testing remaining 20% of data, repeated 100 times). For within-day classification of other imaging runs (e.g., between thirsty/quenched runs, SFO^{GLUT} activation), we trained the classifier on the entirety of data from the two classes (e.g., thirsty vs. quenched, matching the number of observations per class), and tested it on the other runs. For across-day classification, we trained the classifier on the entirety of data from the two classes (e.g., thirsty vs. quenched, matching the number of observations per class) of a given day, and tested it on all runs from the other day's data.

We shuffled time-stamps of population activity by randomly shifting the entire population vector (all simultaneously imaged neurons) in time and classifying thirsty vs. quenched from the shuffled data. We repeated this procedure 100 times per FOV and presented results as the mean across the 100 shuffles per FOV (Figure S2B). Additionally, we shuffled neuron identity 100 times per FOV, classified thirsty vs. quenched from the shuffled data, and presented the results as the mean across the 100 shuffles per FOV (Figure S2B).

In order to estimate what fraction of the population contributed to classification, we sorted neurons by how informative they were for classification (i.e., sorted by their absolute average normalized activity difference across thirsty vs. quenched states, corresponding to classifier weights). We then systematically omitted different fractions of each FOV (in 10% jumps), starting from the most informative neurons. For every omitted population, we performed classification of thirsty vs. quenched (Figure S2C).

To test whether average activity across all neurons per FOV is sufficient for classification, we averaged the activity across neurons for each time-point for each day, in each of the two consecutive days. We then used a procedure that is related to the AODE/Naïve Bayes procedure, as it relies on the empirical mean and STD for estimation of the probability distribution function for each state (see above). We calculated a confidence interval for each state (thirsty vs. quenched) on Day 1 using mean ± 1 STD for that state on Day 1. For each time point on Day 2, we then classified population data as 'correct' if it was within the confidence interval of its respective state (thirsty vs. quenched), and 'incorrect' if it was not (Figure S2E).

To test whether ongoing activity reflects time elapsed, rather than differences across thirsty/quenched states, we imaged during ten-minute periods of disengagement (periods in which water was not available, no cues were presented, and mice did not show obvious licking behavior) between epochs of task engagement, thereby decoupling time elapsed during the session from amount of water consumed. We then compared classification of 20 ITI bins (i.e. concatenated ITI period timecourses from 20 consecutive ITIs) before the disengagement period, to 20 ITI bins after the disengagement period (Figure S3F,G).

Estimation of transitions between states (Figures 3A–C and S3A–C)—We used the same approach to estimate the transition between thirsty/quenched states in behavior

Author Manuscript Author Manuscript Author Manuscript Author Manuscript

(task engagement) in ongoing activity (classification). We represented task engagement as a binary vector with values corresponding either to a correct response to the water cue (1), or an incorrect lack of response to the water cue (0). We represented ongoing activity as classifier probabilities of a thirsty state (range: 1–0). We calculated a running average of both of these vectors using the same window size, and set the crossing of 0.5 as the point of transition from a thirsty to a quenched state, but only if values remained below 0.5 for >50 sec of ITI time (corresponding to ~3 min of 'real time') to enhance robustness of the estimates and avoid noise from rare sporadic changes in estimated states. Importantly, varying the size of the sliding window did not affect our results (Figure S3B). We also used an alternative approach, based on actual pattern similarity. We used the same procedure described for the classifier above, but replaced the classifier with a scaled projection (values: 0–1) of activity from Day 2 onto the thirsty vs. quenched axis from Day 1 (same procedure as in 'Relationship between cue/consumption evoked activity and ongoing activity', below, see also Fig. 7A). This approach yielded similar results to the classifier-based approach (Fig. S3C).

Predicting classifier dynamics from behavioral data (Figures 3D,E and S3D,E)—We predicted ongoing activity dynamics (as reflected in dynamics of classifier state estimation) by a combination of four parameters: (1) cumulative amount of water consumed (coarsely reflecting residual water deficit), (2) pupil diameter (as a proxy for arousal; McGinley et al., 2015), (3) lick response latency on the last rewarded trial, and (4) lick rate on the last rewarded trial ((3) and (4) reflect motivational levels; Berditchevskaia et al., 2016). We performed multiple linear regression using the Matlab function 'regress', and used R^2 values to estimate the fit. We then systematically omitted parameters one by one, and tested how that affected R^2 values.

Relationship between cue/consumption evoked activity and ongoing activity—To correlate cue/consumption evoked activity and differences in ongoing activity, we used z-scored neuronal activity (as described above). First, we subtracted pre-cue values to estimate cue-evoked changes in activity from baseline. We then correlated this to the difference in ongoing activity across states, ΔState, calculated as $\bar{x}_{Thirsty} - \bar{x}_{Quenched}$, were $\bar{x}$ is the mean ongoing activity in a given state (mean of all sub-selected concatenated ITI periods described above; Figure 7B,C).

To assess cue/consumption-evoked changes in classification of thirsty/quenched state from population activity, we trained the classifier on ongoing activity, as described above. We classified all population activity (including during ITIs and during cue presentation periods). We then examined classification in the peri-cue period without any additional normalization or re-zeroing of data (Figure S6A,B).

To project InsCtx population activity patterns onto the axis of thirsty vs. quenched activity (Allen et al., 2019; Li et al., 2016), we defined this axis for each mouse by $\bar{x}_{Thirsty} - \bar{x}_{Quenched}$, where $\bar{x}$ is the population vector of mean ongoing activity in a given state. We projected peri-cue activity onto this axis by calculating the dot product of this vector with the time-varying pattern of InsCtx population activity, x(t). We then scaled

Author Manuscript Author Manuscript Author Manuscript Author Manuscript

values along this axis per mouse, ascribing a value of 1 when x(t) = $\bar{x}_{Thirsty}$, a value of 0 when x(t) = $\bar{x}_{Quenched}$, and intermediate values for patterns that fall between $\bar{x}_{Thirsty}$ and $\bar{x}_{Quenched}$ (Figure 7D,E,G). Note that values below 0 correspond to a position along this axis that is beyond the mean activity of the quenched state (i.e., patterns that are along the thirsty-quenched axis but that are even more dissimilar $\bar{x}_{Thirsty}$ than $\bar{x}_{Quenched}$, and thus correspond to a putative state of overconsumption). We applied the exact same procedure to hungry vs. sated data (Figure 7H). We similarly projected activity onto the High Pupil vs. Low Pupil axis by using the mean population ongoing activity during periods when the pupil size was within the top or bottom 10% of the pupil size distribution, respectively (Fig. 7F; using estimates of mean pupil size during the same set of ITI epochs of ongoing activity as described in Fig. 2D).

To verify that the changes we observed following water cue presentation were not simply due to the larger magnitude of neural responses to water cues vs. other cues, we scaled down the magnitude of the water cue-evoked activity. We did this by scaling the dynamic pattern of responses to the water cue by the mean ratio between lengths of the mean evoked population vectors for the water cue and the neutral cue. This matches population vector lengths, without affecting the pattern of these cue response vectors (Figure S6C).

DATA AND CODE AVAILABILITY

The datasets and code are available upon request to the Lead Contact.

Supplementary Material

Refer to Web version on PubMed Central for supplementary material.

Acknowledgements

We thank M. Barbini, T. Potalla, E. Bamberg, and D. Fleharty for mouse training. We thank the Lowell lab, Andermann lab, S. Khalsa, and D. Nachmani for fruitful discussions. Authors were supported by The Charles A. King Trust Postdoctoral Fellowship, and Boston Nutrition Obesity Research Center P&F 2P30DK046200-26 (YL); NIH K99 HL144923 (JMR); NIH T32 5T32DK007516 (AUS); NSF DGE1745303 (RAE); NIH DP2 DK105570, R01 DK109930, DP1 AT010971, Klarman Family Foundation, McKnight Foundation, Smith Family Foundation, and Pew Scholars Program (MLA); NIH R01s DK075632, DK096010, DK089044, DK111401, and P30s DK046200 and DK057521 (BBL).

References

Abbott SB, Machado NL, Geerling JC, and Saper CB (2016). Reciprocal Control of Drinking Behavior by Median Preoptic Neurons in Mice. J Neurosci 36, 8228–8237. [PubMed: 27488641]

Accolla R, and Carleton A (2008). Internal body state influences topographical plasticity of sensory representations in the rat gustatory cortex. Proc Natl Acad Sci U S A 105, 4010–4015. [PubMed: 18305172]

Allen WE, Chen MZ, Pichamoorthy N, Tien RH, Pachitariu M, Luo L, and Deisseroth K (2019). Thirst regulates motivated behavior through modulation of brainwide neural population dynamics. Science 364, 253. [PubMed: 30948440]

Allen WE, DeNardo LA, Chen MZ, Liu CD, Loh KM, Fenno LE, Ramakrishnan C, Deisseroth K, and Luo L (2017). Thirst-associated preoptic neurons encode an aversive motivational drive. Science 357, 1149–1155. [PubMed: 28912243]

Author Manuscript Author Manuscript Author Manuscript Author Manuscript

Andermann ML, Gilfoy NB, Goldey GJ, Sachdev RN, Wolfel M, McCormick DA, Reid RC, and Levene MJ (2013). Chronic cellular imaging of entire cortical columns in awake mice using microprisms. Neuron 80, 900–913. [PubMed: 24139817]

Andermann ML, Kerlin AM, Roumis DK, Glickfeld LL, and Reid RC (2011). Functional specialization of mouse higher visual cortical areas. Neuron 72, 1025–1039. [PubMed: 22196337]

Andermann ML, and Lowell BB (2017). Toward a Wiring Diagram Understanding of Appetite Control. Neuron 95, 757–778. [PubMed: 28817798]

Aponte Y, Atasoy D, and Sternson SM (2011). AGRP neurons are sufficient to orchestrate feeding behavior rapidly and without training. Nat Neurosci 14, 351–355. [PubMed: 21209617]

Arieli A, Sterkin A, Grinvald A, and Aertsen A (1996). Dynamics of ongoing activity: explanation of the large variability in evoked cortical responses. Science 273, 1868–1871. [PubMed: 8791593]

Asaad WF, and Eskandar EN (2008). A flexible software tool for temporally-precise behavioral control in Matlab. J Neurosci Methods 174, 245–258. [PubMed: 18706928]

Augustine V, Gokce SK, Lee S, Wang B, Davidson TJ, Reimann F, Gribble F, Deisseroth K, Lois C, and Oka Y (2018a). Hierarchical neural architecture underlying thirst regulation. Nature 555, 204–209. [PubMed: 29489747]

Augustine V, Gokce SK, and Oka Y (2018b). Peripheral and Central Nutrient Sensing Underlying Appetite Regulation. Trends Neurosci 41, 526–539. [PubMed: 29914721]

Barrett LF, and Simmons WK (2015). Interoceptive predictions in the brain. Nat Rev Neurosci 16, 419–429. [PubMed: 26016744]

Baxter MG, and Murray EA (2002). The amygdala and reward. Nat Rev Neurosci 3, 563–573. [PubMed: 12094212]

Becker CA, Schmalzle R, Flaisch T, Renner B, and Schupp HT (2015). Thirst and the state-dependent representation of incentive stimulus value in human motive circuitry. Soc Cogn Affect Neurosci 10, 1722–1729. [PubMed: 25971601]

Berditchevskaia A, Caze RD, and Schultz SR (2016). Performance in a GO/NOGO perceptual task reflects a balance between impulsive and instrumental components of behaviour. Sci Rep 6, 27389. [PubMed: 27272438]

Betley JN, Cao ZF, Ritola KD, and Sternson SM (2013). Parallel, redundant circuit organization for homeostatic control of feeding behavior. Cell 155, 1337–1350. [PubMed: 24315102]

Betley JN, Xu S, Cao ZF, Gong R, Magnus CJ, Yu Y, and Sternson SM (2015). Neurons for hunger and thirst transmit a negative-valence teaching signal. Nature 521, 180–185. [PubMed: 25915020]

Beyeler A, Namburi P, Glober GF, Simonnet C, Calhoon GG, Conyers GF, Luck R, Wildes CP, and Tye KM (2016). Divergent Routing of Positive and Negative Information from the Amygdala during Memory Retrieval. Neuron 90, 348–361. [PubMed: 27041499]

Bonin V, Histed MH, Yurgenson S, and Reid RC (2011). Local diversity and fine-scale organization of receptive fields in mouse visual cortex. J Neurosci 31, 18506–18521. [PubMed: 22171051]

Burgess CR, Ramesh RN, Sugden AU, Levandowski KM, Minnig MA, Fenselau H, Lowell BB, and Andermann ML (2016). Hunger-Dependent Enhancement of Food Cue Responses in Mouse Postrhinal Cortex and Lateral Amygdala. Neuron 91, 1154–1169. [PubMed: 27523426]

Chen Y, Lin YC, Zimmerman CA, Essner RA, and Knight ZA (2016). Hunger neurons drive feeding through a sustained, positive reinforcement signal. Elife 5.

Contreras M, Ceric F, and Torrealba F (2007). Inactivation of the interoceptive insula disrupts drug craving and malaise induced by lithium. Science 318, 655–658. [PubMed: 17962567]

Craig AD (2003). Interoception: the sense of the physiological condition of the body. Curr Opin Neurobiol 13, 500–505. [PubMed: 12965300]

Critchley HD, and Harrison NA (2013). Visceral influences on brain and behavior. Neuron 77, 624–638. [PubMed: 23439117]

de Araujo IE, Gutierrez R, Oliveira-Maia AJ, Pereira A Jr., Nicolelis MA, and Simon SA (2006). Neural ensemble coding of satiety states. Neuron 51, 483–494. [PubMed: 16908413]

de Araujo IE, Kringelbach ML, Rolls ET, and McGlone F (2003). Human cortical responses to water in the mouth, and the effects of thirst. J Neurophysiol 90, 1865–1876. [PubMed: 12773496]

Author Manuscript Author Manuscript Author Manuscript Author Manuscript

Domingos AI, Vaynshteyn J, Voss HU, Ren X, Gradinaru V, Zang F, Deisseroth K, de Araujo IE, and Friedman J (2011). Leptin regulates the reward value of nutrient. Nat Neurosci 14, 1562–1568. [PubMed: 22081158]

Driscoll LN, Pettit NL, Minderer M, Chettih SN, and Harvey CD (2017). Dynamic Reorganization of Neuronal Activity Patterns in Parietal Cortex. Cell 170, 986–999 e916. [PubMed: 28823559]

Egan G, Silk T, Zamarripa F, Williams J, Federico P, Cunnington R, Carabott L, Blair-West J, Shade R, McKinley M, et al. (2003). Neural correlates of the emergence of consciousness of thirst. Proc Natl Acad Sci U S A 100, 15241–15246. [PubMed: 14657368]

Euston DR, Gruber AJ, and McNaughton BL (2012). The role of medial prefrontal cortex in memory and decision making. Neuron 76, 1057–1070. [PubMed: 23259943]

Fazeli S, and Buchel C (2018). Pain-Related Expectation and Prediction Error Signals in the Anterior Insula Are Not Related to Aversiveness. J Neurosci 38, 6461–6474. [PubMed: 29934355]

Frank S, Kullmann S, and Veit R (2013). Food related processes in the insular cortex. Front Hum Neurosci 7, 499. [PubMed: 23986683]

Friedman J, Hastie T, and Tibshirani R (2010). Regularization Paths for Generalized Linear Models via Coordinate Descent. Journal of statistical software 33, 1–22. [PubMed: 20808728]

Garcia-Cordero I, Sedeno L, de la Fuente L, Slachevsky A, Forno G, Klein F, Lillo P, Ferrari J, Rodriguez C, Bustin J, et al. (2016). Feeling, learning from and being aware of inner states: interoceptive dimensions in neurodegeneration and stroke. Philos Trans R Soc Lond B Biol Sci 371.

Gardner MP, and Fontanini A (2014). Encoding and tracking of outcome-specific expectancy in the gustatory cortex of alert rats. J Neurosci 34, 13000–13017. [PubMed: 25253848]

Gehrlach DA, Dolensek N, Klein AS, Roy Chowdhury R, Matthys A, Junghanel M, Gaitanos TN, Podgornik A, Black TD, Reddy Vaka N, et al. (2019). Aversive state processing in the posterior insular cortex. Nat Neurosci 22, 1424–1437. [PubMed: 31455886]

Gizowski C, and Bourque CW (2018). The neural basis of homeostatic and anticipatory thirst. Nature reviews Nephrology 14, 11–25. [PubMed: 29129925]

Gogolla N (2017). The insular cortex. Curr Biol 27, R580–R586. [PubMed: 28633023]

Grewe BF, Grundemann J, Kitch LJ, Lecoq JA, Parker JG, Marshall JD, Larkin MC, Jercog PE, Grenier F, Li JZ, et al. (2017). Neural ensemble dynamics underlying a long-term associative memory. Nature 543, 670–675. [PubMed: 28329757]

Grossman SE, Fontanini A, Wieskopf JS, and Katz DB (2008). Learning-related plasticity of temporal coding in simultaneously recorded amygdala-cortical ensembles. J Neurosci 28, 2864–2873. [PubMed: 18337417]

Grundemann J, Bitterman Y, Lu T, Krabbe S, Grewe BF, Schnitzer MJ, and Luthi A (2019). Amygdala ensembles encode behavioral states. Science 364.

Hashikawa Y, Hashikawa K, Falkner AL, and Lin D (2017). Ventromedial Hypothalamus and the Generation of Aggression. Front Syst Neurosci 11, 94. [PubMed: 29375329]

Hollis JH, McKinley MJ, D'Souza M, Kampe J, and Oldfield BJ (2008). The trajectory of sensory pathways from the lamina terminalis to the insular and cingulate cortex: a neuroanatomical framework for the generation of thirst. Am J Physiol Regul Integr Comp Physiol 294, R1390–1401. [PubMed: 18234743]

Huerta CI, Sarkar PR, Duong TQ, Laird AR, and Fox PT (2014). Neural bases of food perception: coordinate-based meta-analyses of neuroimaging studies in multiple modalities. Obesity 22, 1439–1446. [PubMed: 24174404]

Hull CL (1943). Principles of behavior: an introduction to behavior theory. D. Appleton-century company. Inc, New York, 85–101.

Johnson AK, and Thunhorst RL (1997). The neuroendocrinology of thirst and salt appetite: visceral sensory signals and mechanisms of central integration. Front Neuroendocrinol 18, 292–353. [PubMed: 9237080]

Juechems K, and Summerfield C (2019). Where Does Value Come From? Trends Cogn Sci 23, 836–850. [PubMed: 31494042]

Katz DB, Simon SA, and Nicolelis MA (2001). Dynamic and multimodal responses of gustatory cortical neurons in awake rats. J Neurosci 21, 4478–4489. [PubMed: 11404435]

Author Manuscript Author Manuscript Author Manuscript Author Manuscript

Keramati M, and Gutkin B (2014). Homeostatic reinforcement learning for integrating reward collection and physiological stability. Elife 3.

Khalsa SS, Adolphs R, Cameron OG, Critchley HD, Davenport PW, Feinstein JS, Feusner JD, Garfinkel SN, Lane RD, Mehling WE, et al. (2018). Interoception and Mental Health: A Roadmap. Biological psychiatry Cognitive neuroscience and neuroimaging 3, 501–513. [PubMed: 29884281]

Kim J, Pignatelli M, Xu S, Itohara S, and Tonegawa S (2016). Antagonistic negative and positive neurons of the basolateral amygdala. Nat Neurosci 19, 1636–1646. [PubMed: 27749826]

Klavir O, Genud-Gabai R, and Paz R (2013). Functional connectivity between amygdala and cingulate cortex for adaptive aversive learning. Neuron 80, 1290–1300. [PubMed: 24314732]

Kohl J, Babayan BM, Rubinstein ND, Autry AE, Marin-Rodriguez B, Kapoor V, Miyamishi K, Zweifel LS, Luo L, Uchida N, et al. (2018). Functional circuit architecture underlying parental behaviour. Nature 556, 326–331. [PubMed: 29643503]

Krashes MJ, Koda S, Ye C, Rogan SC, Adams AC, Cusher DS, Maratos-Flier E, Roth BL, and Lowell BB (2011). Rapid, reversible activation of AgRP neurons drives feeding behavior in mice. J Clin Invest 121, 1424–1428. [PubMed: 21364278]

Kurt G, Woodworth HL, Fowler S, Bugescu R, and Leinninger GM (2018). Activation of lateral hypothalamic area neurotensin-expressing neurons promotes drinking. Neuropharmacology.

Kusumoto-Yoshida I, Liu H, Chen BT, Fontanini A, and Bonci A (2015). Central role for the insular cortex in mediating conditioned responses to anticipatory cues. Proc Natl Acad Sci U S A 112, 1190–1195. [PubMed: 25583486]

Kyriazi P, Headley DB, and Pare D (2018). Multi-dimensional Coding by Basolateral Amygdala Neurons. Neuron 99, 1315–1328 e1315. [PubMed: 30146300]

Lavi K, Jacobson GA, Rosenblum K, and Luthi A (2018). Encoding of Conditioned Taste Aversion in Cortico-Amygdala Circuits. Cell Rep 24, 278–283. [PubMed: 29996089]

Leib DE, Zimmerman CA, Poormoghaddam A, Huey EL, Ahn JS, Lin YC, Tan CL, Chen Y, and Knight ZA (2017). The Forebrain Thirst Circuit Drives Drinking through Negative Reinforcement. Neuron 96, 1272–1281 e1274. [PubMed: 29268095]

Levitan D, Lin J-Y, Wachutka J, Mukherjee N, Nelson SB, and Katz DB (2019a). Single and population coding of taste in the gustatory-cortex of awake mice. bioRxiv, 575522.

Levitan D, Lin JY, Wachutka J, Mukherjee N, Nelson SB, and Katz DB (2019b). Single and population coding of taste in the gustatory cortex of awake mice. J Neurophysiol 122, 1342–1356. [PubMed: 31339800]

Li N, Daie K, Svoboda K, and Druckmann S (2016). Robust neuronal dynamics in premotor cortex during motor planning. Nature 532, 459–464. [PubMed: 27074502]

Livneh Y, Ramesh RN, Burgess CR, Levandowski KM, Madara JC, Fenselau H, Goldey GJ, Diaz VE, Jikomes N, Resch JM, et al. (2017). Homeostatic circuits selectively gate food cue responses in insular cortex. Nature 546, 611–616. [PubMed: 28614299]

Lowell BB (2019). New Neuroscience of Homeostasis and Drives for Food, Water, and Salt. N Engl J Med 380, 459–471. [PubMed: 30699320]

Lutas A, Kucukdereli H, Alturkistani O, Carty C, Sugden AU, Fernando K, Diaz V, Flores-Maldonado V, and Andermann ML (2019). State-specific gating of salient cues by midbrain dopaminergic input to basal amygdala. Nat Neurosci.

Mandelblat-Cerf Y, Kim A, Burgess CR, Subramanian S, Tannous BA, Lowell BB, and Andermann ML (2017). Bidirectional Anticipation of Future Osmotic Challenges by Vasopressin Neurons. Neuron 93, 57–65. [PubMed: 27989461]

Marciante AB, Wang LA, Farmer GE, and Cunningham JT (2019). Selectively Inhibiting the Median Preoptic Nucleus Attenuates Angiotensin II and Hyperosmotic-Induced Drinking Behavior and Vasopressin Release in Adult Male Rats. eNeuro 6.

McGinley MJ, Vinck M, Reimer J, Batista-Brito R, Zagha E, Cadwell CR, Tolias AS, Cardin JA, and McCormick DA (2015). Waking State: Rapid Variations Modulate Neural and Behavioral Responses. Neuron 87, 1143–1161. [PubMed: 26402600]

McKinley MJ, Denton DA, Ryan PJ, Yao ST, Stefanidis A, and Oldfield BJ (2019). From sensory circumventricular organs to cerebral cortex: Neural pathways controlling thirst and hunger. J Neuroendocrinol 31, e12689. [PubMed: 30672620]

Author Manuscript Author Manuscript Author Manuscript Author Manuscript

Meier L, Federspiel A, Jann K, Wiest R, Strik W, and Dierks T (2018). Thirst-Dependent Activity of the Insular Cortex Reflects its Emotion-Related Subdivision: A Cerebral Blood Flow Study. Neuroscience 383, 170–177. [PubMed: 29704610]

Morrison SE, and Salzman CD (2010). Re-valuing the amygdala. Curr Opin Neurobiol 20, 221–230. [PubMed: 20299204]

Mukamel EA, Nimmerjahn A, and Schnitzer MJ (2009). Automated analysis of cellular signals from large-scale calcium imaging data. Neuron 63, 747–760. [PubMed: 19778505]

Musall S, Kaufman MT, Juavinett AL, Gluf S, and Churchland AK (2019). Single-trial neural dynamics are dominated by richly varied movements. Nat Neurosci 22, 1677–1686. [PubMed: 31551604]

Namburi P, Beyeler A, Yorozu S, Calhoon GG, Halbert SA, Wichmann R, Holden SS, Mertens KL, Anahtar M, Felix-Ortiz AC, et al. (2015). A circuit mechanism for differentiating positive and negative associations. Nature 520, 675–678. [PubMed: 25925480]

Naqvi NH, Gaznick N, Tranel D, and Bechara A (2014). The insula: a critical neural substrate for craving and drug seeking under conflict and risk. Ann N Y Acad Sci 1316, 53–70. [PubMed: 24690001]

Niell CM, and Stryker MP (2010). Modulation of visual responses by behavioral state in mouse visual cortex. Neuron 65, 472–479. [PubMed: 20188652]

Oka Y, Ye M, and Zuker CS (2015). Thirst driving and suppressing signals encoded by distinct neural populations in the brain. Nature 520, 349–352. [PubMed: 25624099]

Owens AP, Allen M, Ondobaka S, and Friston KJ (2018). Interoceptive inference: From computational neuroscience to clinic. Neurosci Biobehav Rev 90, 174–183. [PubMed: 29694845]

Paulus MP, Feinstein JS, and Khalsa SS (2019). An Active Inference Approach to Interoceptive Psychopathology. Annual review of clinical psychology 15, 97–122.

Quadt L, Critchley HD, and Garfinkel SN (2018). The neurobiology of interoception in health and disease. Ann N Y Acad Sci 1428, 112–128. [PubMed: 29974959]

Ramesh RN, Burgess CR, Sugden AU, Gyetvan M, and Andermann ML (2018). Intermingled Ensembles in Visual Association Cortex Encode Stimulus Identity or Predicted Outcome. Neuron 100, 900–915 e909. [PubMed: 30318413]

Resch JM, Fenselau H, Madara JC, Wu C, Campbell JN, Lyubetskaya A, Dawes BA, Tsai LT, Li MM, Livneh Y, et al. (2017). Aldosterone-Sensing Neurons in the NTS Exhibit State-Dependent Pacemaker Activity and Drive Sodium Appetite via Synergy with Angiotensin II Signaling. Neuron 96, 190–206 e197. [PubMed: 28957668]

Salkoff DB, Zagha E, McCarthy E, and McCormick DA (2019). Movement and Performance Explain Widespread Cortical Activity in a Visual Detection Task. Cereb Cortex.

Samuelsen CL, Gardner MP, and Fontanini A (2012). Effects of cue-triggered expectation on cortical processing of taste. Neuron 74, 410–422. [PubMed: 22542192]

Samuelsen CL, Gardner MP, and Fontanini A (2013). Thalamic contribution to cortical processing of taste and expectation. J Neurosci 33, 1815–1827. [PubMed: 23365221]

Saper CB (2002). The central autonomic nervous system: conscious visceral perception and autonomic pattern generation. Annu Rev Neurosci 25, 433–469. [PubMed: 12052916]

Stapleton JR, Lavine ML, Wolpert RL, Nicolelis MA, and Simon SA (2006). Rapid taste responses in the gustatory cortex during licking. J Neurosci 26, 4126–4138. [PubMed: 16611830]

Sternson SM, and Eiselt AK (2017). Three Pillars for the Neural Control of Appetite. Annu Rev Physiol 79, 401–423. [PubMed: 27912679]

Stringer C, Pachitariu M, Steinmetz N, Reddy CB, Carandini M, and Harris KD (2019). Spontaneous behaviors drive multidimensional, brainwide activity. Science 364, 255. [PubMed: 31000656]

Sugden LA, Atkinson EG, Fischer AP, Rong S, Henn BM, and Ramachandran S (2018). Localization of adaptive variants in human genomes using averaged one-dependence estimation. Nat Commun 9, 703. [PubMed: 29459739]

Tan CL, Cooke EK, Leib DE, Lin YC, Daly GE, Zimmerman CA, and Knight ZA (2016). Warm-Sensitive Neurons that Control Body Temperature. Cell 167, 47–59 e15. [PubMed: 27616062]

Author Manuscript Author Manuscript Author Manuscript Author Manuscript

Tataranni PA, Gautier JF, Chen K, Uecker A, Bandy D, Salbe AD, Pratley RE, Lawson M, Reiman EM, and Ravussin E (1999). Neuroanatomical correlates of hunger and satiation in humans using positron emission tomography. Proc Natl Acad Sci U S A 96, 4569–4574. [PubMed: 10200303]

Vincis R, and Fontanini A (2016). Associative learning changes cross-modal representations in the gustatory cortex. Elife 5.

Webb GI, Boughton JR, and Wang Z (2005). Not So Naive Bayes: Aggregating One-Dependence Estimators. Machine Learning 58, 5–24.

Wittmann M (2013). The inner sense of time: how the brain creates a representation of duration. Nat Rev Neurosci 14, 217–223. [PubMed: 23403747]

Wolff SB, and Olveczky BP (2018). The promise and perils of causal circuit manipulations. Curr Opin Neurobiol 49, 84–94. [PubMed: 29414070]

Zhang X, and Li B (2018). Population coding of valence in the basolateral amygdala. Nat Commun 9, 5195. [PubMed: 30518754]

Zimmerman CA, Leib DE, and Knight ZA (2017). Neural circuits underlying thirst and fluid homeostasis. Nat Rev Neurosci 18, 459–469. [PubMed: 28638120]

Zimmerman CA, Lin YC, Leib DE, Guo L, Huey EL, Daly GE, Chen Y, and Knight ZA (2016). Thirst neurons anticipate the homeostatic consequences of eating and drinking. Nature 537, 680–684. [PubMed: 27487211]

Ziv Y, Burns LD, Cocker ED, Hamel EO, Ghosh KK, Kitch LJ, El Gamal A, and Schnitzer MJ (2013). Long-term dynamics of CA1 hippocampal place codes. Nat Neurosci 16, 264–266. [PubMed: 23396101]

Author Manuscript Author Manuscript Author Manuscript Author Manuscript

Highlights:

- InsCtx ongoing activity patterns reflect current bodily state, not behavioral state
- Hypothalamic hunger/thirst neurons gate InsCtx responses to food/water cues
- Hypothalamic hunger/thirst neurons do not gate InsCtx ongoing activity
- Food/water cues drive transient “simulations” of future bodily states in InsCtx

Author Manuscript Author Manuscript Author Manuscript Author Manuscript

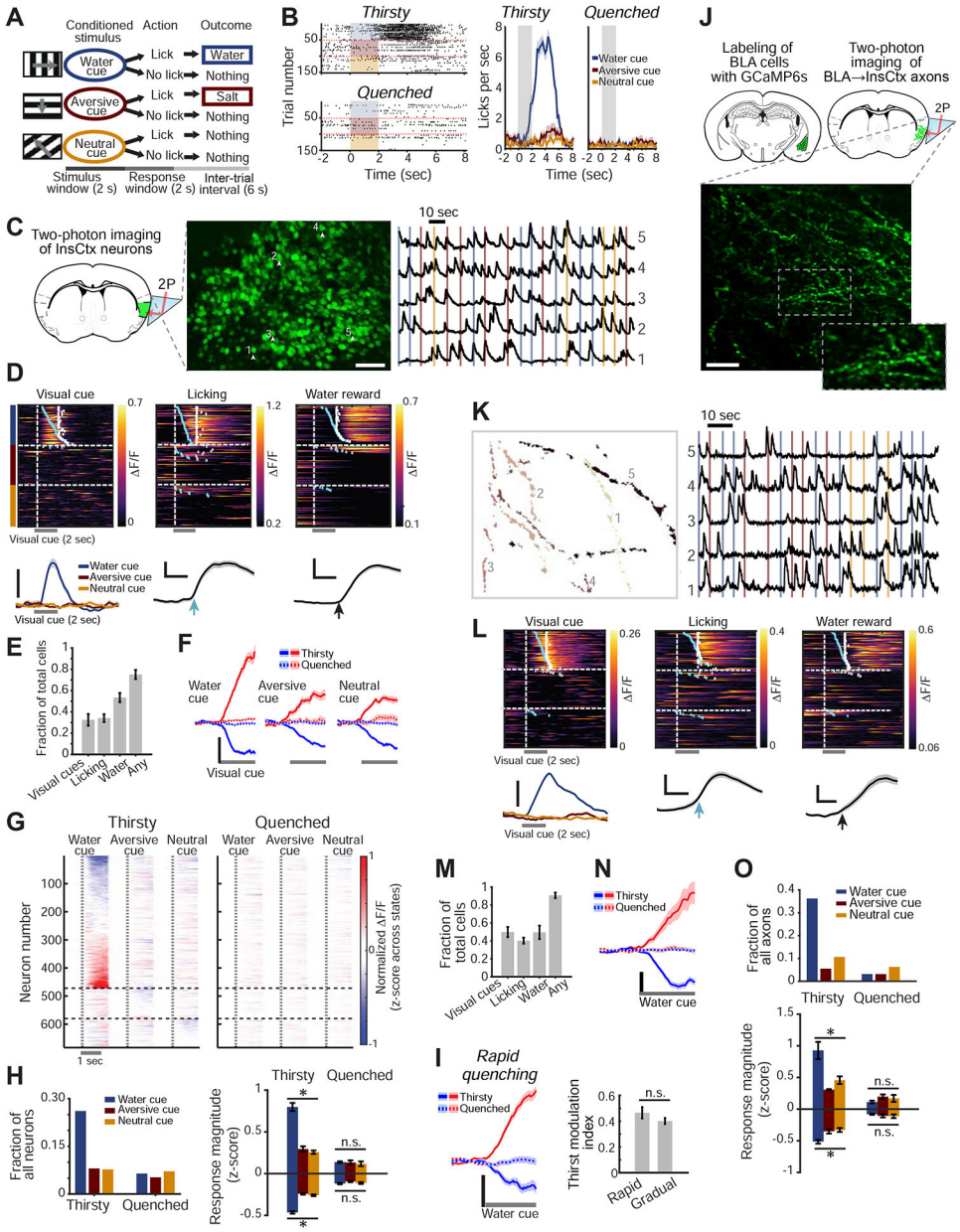

Figure 1: Thirst-Dependent Bias to Water Cues in InsCtx Neurons and BLA→InsCtx Axons

A. Schematic of visual discrimination task.

B. Example task-related licking behavior across thirsty and quenched states. *Left*: lick rasters. Shading: 2 sec visual cue. *Right*: mean±s.e.m. of 50–55 cue presentations.

C. Two-photon calcium imaging of InsCtx through a microprism. *Left*: schematic coronal brain section and approach. *Middle*: example two-photon image of GCaMP6f-expressing neurons. Numbers correspond to traces in right panel. Scale bar: 100 μm. *Right*: normalized fractional change in fluorescence, ΔF/F. Vertical lines: cue onsets (colors as in **A**-**B**).

D. Example single neurons with time-locked responses to water cue, licking, or water. *Top*: heatmaps (rows: trials). Blue ticks: lick-bout onset; white ticks: water delivery. *Bottom*: average responses of the same neurons. Scale bars: 20% ΔF/F; 1 sec (*middle, right*).

Author Manuscript Author Manuscript Author Manuscript Author Manuscript

E. Fraction of neurons that responded to task events (n=1953 neurons from 12 fields-of-view [FOVs] in 9 mice). Values: mean±s.e.m. across FOVs.

F. Average population responses of neurons significantly activated (red) or suppressed (blue) by the 3 visual cues across states. Scale bar: 0.2 normalized ΔF/F (z-score across states). Values: mean±s.e.m; n=581, 204 and 221 neurons responding to the water, aversive and neutral cues, respectively (9 mice).

G. Heatmap of average neuronal responses to the 3 visual cues during thirsty and quenched states for all cue-responsive neurons. Vertical dashed lines: visual cue onset. Horizontal dashed lines: separation between sets of neurons, grouped by the cue that evoked the strongest response.

H. Quantitative analyses of cue-responsive neurons. *Left*: fraction of all recorded neurons (n=1953 neurons from 9 mice) responsive to each visual cue. *Right*: average response magnitude across thirsty and quenched states. Within state: *$p<2\times10^{-12}$, n.s.: not significant ($p>0.13$), Kruskal-Wallis test. Pairwise comparisons (Thirsty): water vs. aversive/neutral cue: $p\leq1.3\times10^{-6}$, aversive vs. neutral cue: $p\geq0.22$. Pairwise comparisons (Thirsty vs. Quenched): $p\leq5.5\times10^{-4}$ for all 3 cues, Mann-Whitney test (neurons with significant responses to the water, aversive and neutral cues: suppressed: n= 324, 175 and 180, respectively; activated: n= 257, 29 and 41; 12 FOVs, 9 mice).

I. Comparison of cue responses between rapid and gradual quenching. *Left*: average population responses to the water cue across states following a rapid quenching protocol. *Right*: thirst modulation index for rapid and gradual quenching protocols (p=0.2, Mann-Whitney test, n=100 neurons from 3 mice for rapid quenching, n=387 neurons from 6 mice for gradual quenching).

J. Two-photon imaging of BLA→InsCtx axons. *Top*: approach. *Bottom*: example two-photon image. Scale bar: 20 μm.

K. Five example axons from **J**. *Left*: regions-of-interest (colors denote different axons). *Right*: normalized ΔF/F. Vertical lines: cue onsets.

L. Example single axons with time-locked responses to different events: water cue, licking, or water. *Top*: heatmaps (rows: trials). Blue ticks: times of lick-bout onset; white ticks: times of water delivery. *Bottom*: average responses of the same axons. Scale bars: 10% ΔF/F, 1 sec (*middle, right*).

M. Fraction of axons that responded to task events (n=257 axons imaged from 5 FOVs in 3 mice). Values: mean±s.e.m. across FOVs.

N. Average population responses of BLA→InsCtx axons to the water cue across states. Scale bar: 0.2 normalized ΔF/F (z-score across states). Values: mean±s.e.m; n=92 cue-responsive axons.

O. Quantitative analyses of cue-responsive axons. *Top*: fraction of all recorded axons (n=257) responsive to each visual cue. Within state: *$p\leq0.01$. n.s.: not significant ($p>0.38$, Quenched), Kruskal-Wallis test. Pairwise comparisons (Thirsty): water vs. aversive/neutral cue: $p\leq0.03$, aversive vs. neutral cue: $p\geq0.4$. Pairwise comparisons (Thirsty vs. Quenched): $p\leq0.007$ for all 3 cues (except activated aversive cue responses with small sample size), Mann-Whitney test (axons responding to the water, aversive and neutral cues: suppressed: n= 66, 12 and 13, activated: n= 26, 2 and 14, respectively; 5 FOVs from 3 mice).

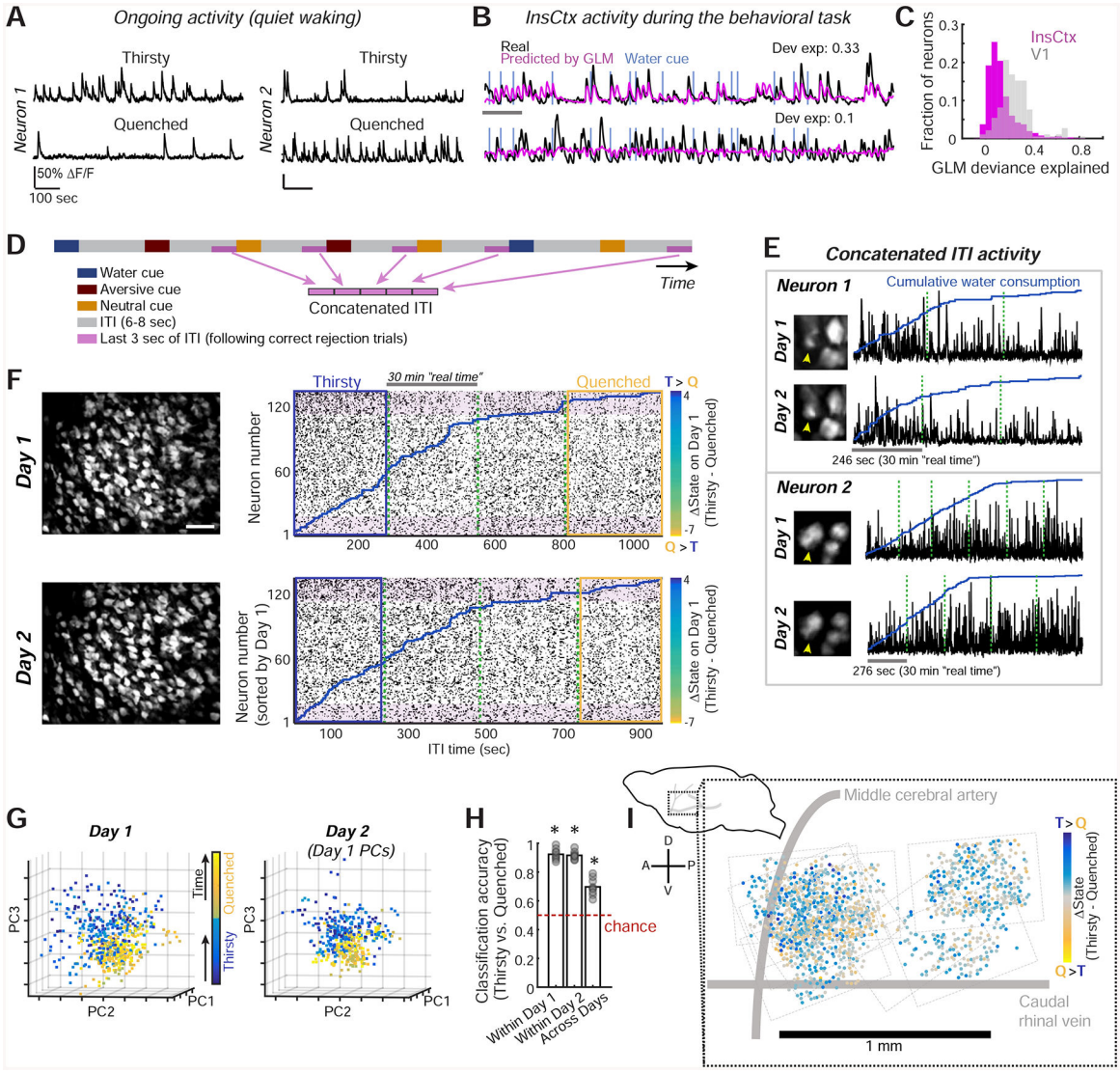

Figure 2: Thirst-Related Ongoing Activity Patterns in InsCtx

A. Example activity of two InsCtx neurons during periods of quiet waking. Scale bars: 50% ΔF/F, 100 sec.

B. Activity of example neurons that are well fit (fractional deviance explained: 0.33) or poorly fit (0.1) by the GLM. Scale bar: 60 sec. Dev. exp.: deviance explained.

C. Distribution of GLM fits for InsCtx vs. V1 neuron activity during the visual discrimination task.

D. Schematic of the approach for analyzing ongoing activity, restricted to a subset of ITIs not associated with any overt behaviors.

E. Example ongoing activity (concatenated ITIs) of two InsCtx neurons across two days. Green dashed lines separate consecutive 30 min imaging sessions.

F. Example ongoing activity of a population of InsCtx neurons. *Left*: two-photon images across two days. Scale bar: 100 μm. *Right*: ongoing activity of the same neurons across the two days. Blue lines: cumulative water consumption during the visual discrimination task. Green dashed lines: separation between consecutive 30 min sessions. Shaded pink rectangles

Author Manuscript Author Manuscript Author Manuscript Author Manuscript

Author Manuscript Author Manuscript Author Manuscript Author Manuscript

highlight sets of neurons with similar changes in activity across states on both days. Blue/yellow rectangles: thirsty/quenched sessions in **G**. Neurons were sorted by the difference in ongoing activity in Thirsty vs. Quenched states on Day 1 (see colorbars).

G. Projection of population activity on the first three PCs for the experiment in **F**. Note that Day 2 data was projected onto Day 1 PCs.

H. Classification of ongoing activity within day and across days. Classifier was trained on Thirsty and Quenched epochs (blue and yellow rectangles in **F**). *$p \leq 0.003$, t-test vs. chance, n=9 FOVs.

I. *Left*: schematic side view of mouse brain. *Right*: anatomical location of all imaged neurons (dots) across mice. Dashed rectangles: borders of each FOV. A: anterior, P: posterior, D: dorsal, V: ventral.

Author Manuscript Author Manuscript Author Manuscript Author Manuscript

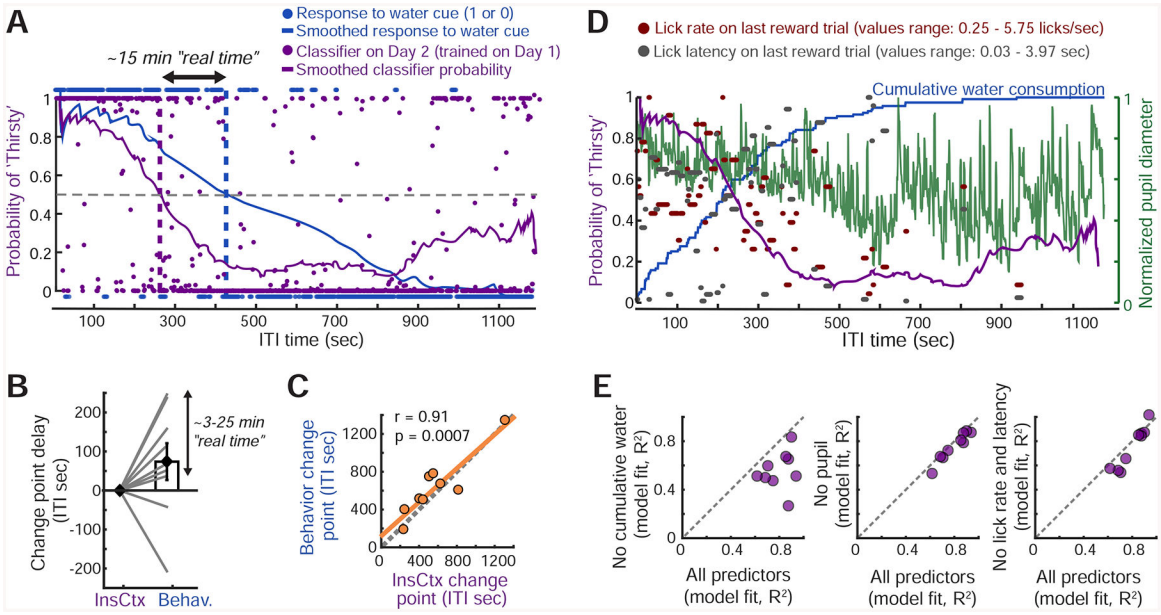

Figure 3: InsCtx Ongoing Activity Reflects Water Consumed, Rather than Arousal or Behavior

A. Classification of hydration state from ongoing activity of a population of InsCtx neurons at each time point in a behavioral session. The classifier was trained on the previous day's ongoing activity patterns during Thirsty vs. Quenched epochs. Dashed purple line: change point of the classifier. Dashed blue line: actual change in behavioral state (task engagement). Dashed gray line: 50% probability of classification as Thirsty. See Fig. S3A.

B. Difference between change points in the transition from Thirsty to Quenched for the InsCtx activity-based classifier and for behavioral performance in each experiment.

C. Correlation between the two change points across all experiments.

D. Classifier estimates of Thirsty/Quenched states from ongoing activity (purple) were modeled using multiple behavioral variables.

E. Model fit using all or subsets of these variables. See Fig. S3C,D.

Author Manuscript Author Manuscript Author Manuscript Author Manuscript

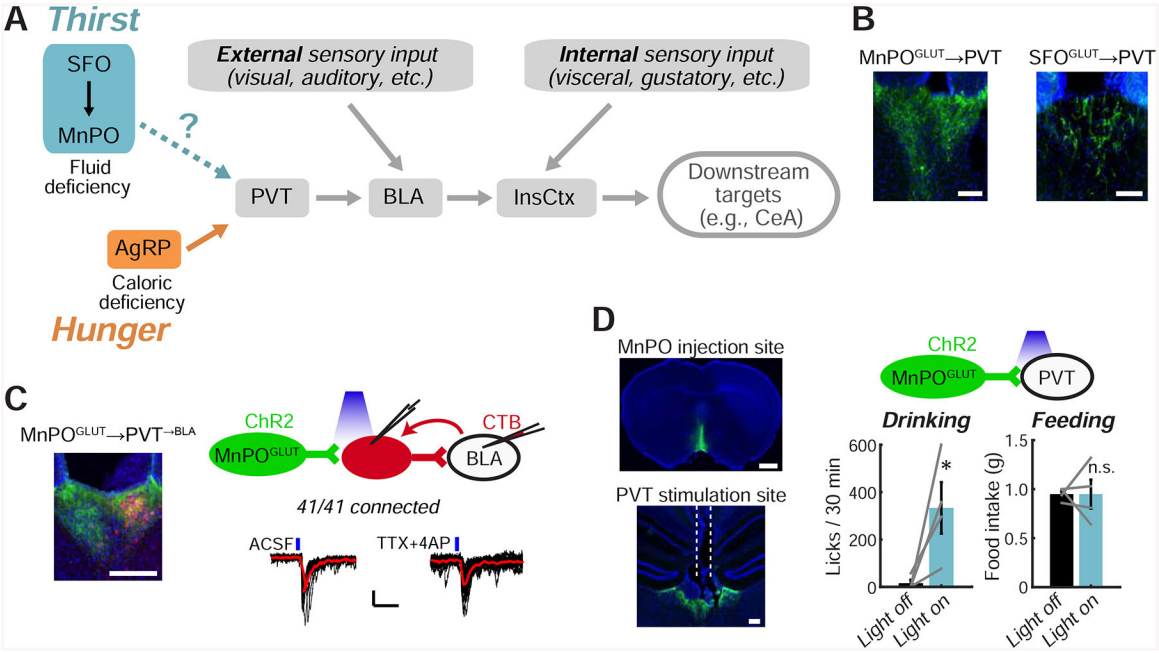

Figure 4: Convergence of Hypothalamic Hunger and Thirst Neurons on a Pathway to InsCtx

A. Potential convergence of AgRP hunger neurons with SFO^{GLUT}/MnPO^{GLUT} thirst neurons onto a pathway to InsCtx.

B. ChR2-YFP-expressing SFO^{GLUT} and MnPO^{GLUT} axons in PVT. Scale bars: 100 μm.

C. *Left*: CTB-labeled PVT→BLA neurons (red) intermingled with MnPO^{GLUT} axons (green). Scale bar: 200 μm. *Top right*: schematic of CRACM from MnPO^{GLUT} neurons to PVT→BLA neurons. *Bottom right*: example recording of MnPO^{GLUT} inputs to PVT→BLA neurons. Black lines: individual sweeps; red line: average of 15 sweeps; blue lines: blue light stimulations. Scale bars: 10 pA, 50 ms. Application of TTX+4AP did not abolish light-evoked synaptic currents, indicating monosynaptic connectivity.

D. Optogenetic activation of MnPO^{GLUT} terminals in PVT. *Left*: example injection site and fiber site (dashed white lines). Scale bars: 1 mm (top), 200 μm (bottom). *Top right*: schematic. *Bottom right*: MnPO^{GLUT}→PVT axon terminal stimulation induced drinking but not feeding (2 hours of post-fast refeeding). *p=0.03, n.s.: not significant, p=0.4.

Author Manuscript Author Manuscript Author Manuscript Author Manuscript

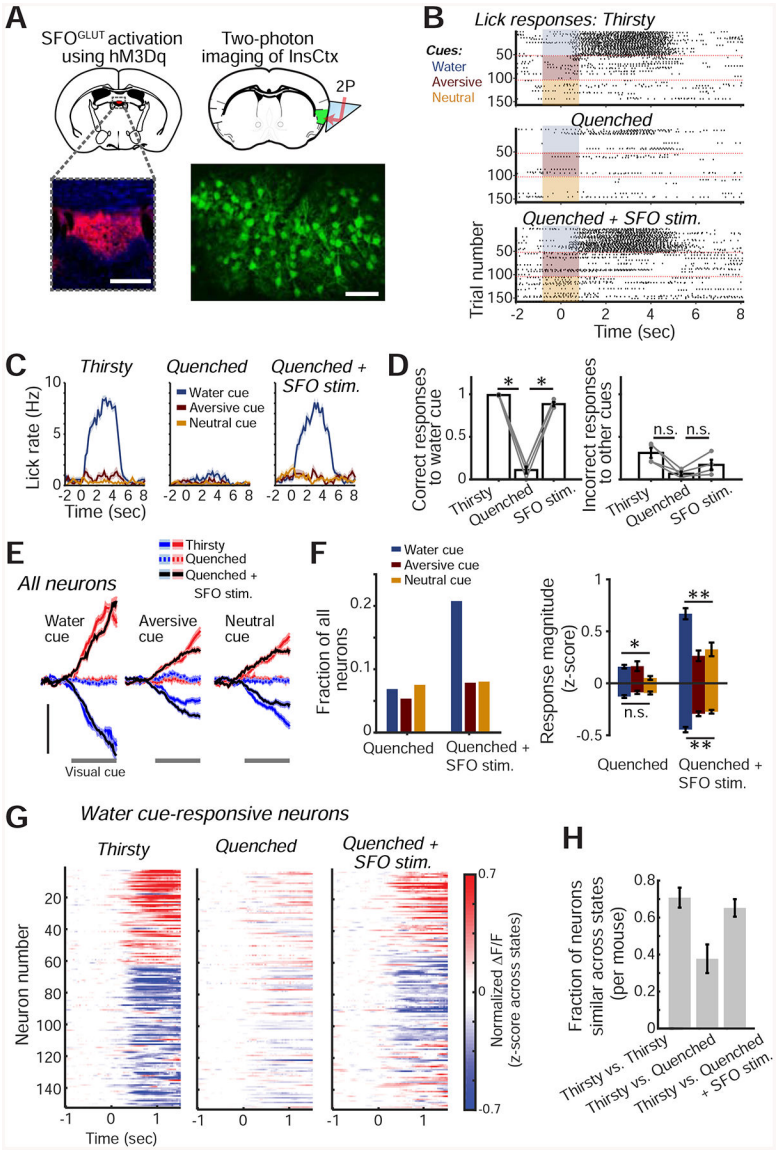

Figure 5: SFO^{GLUT} Activation Mimics Thirst Behaviorally and in InsCtx Cue Responses

A. Experimental approach for chemogenetic activation of SFO^{GLUT} neurons (*top left*) while imaging InsCtx (*top right*). *Bottom left*: image of SFO showing hM3Dq-mCherry expression. Scale bar: 200 μm. *Bottom right*: two-photon image of InsCtx during SFO^{GLUT} activation. Scale bar: 100 μm.

B. Example lick rasters during the visual discrimination task.

C. Lick rates (mean±s.e.m) for data in **B**.

D. Summary of behavior across mice (n=4). Correct water cue responses across conditions: $p=5.2\times10^{-9}$ (one-way ANOVA), pairwise comparisons: $p\leq0.02$ (paired t-test). Incorrect responses to other cues across conditions: p=0.02 (one-way ANOVA), Thirsty vs. Quenched: p=0.02 (paired t-test), Quenched vs. SFO^{GLUT} stim: p=0.07 (paired t-test), Thirsty vs. SFO^{GLUT} stim: p=0.16 (paired t-test). All tests include Holm-Bonferroni correction for multiple comparisons.

Author Manuscript Author Manuscript Author Manuscript Author Manuscript

E. Average population responses of all imaged neurons activated (red) or suppressed (blue) by the 3 visual cues. Scale bars: 0.2 normalized ΔF/F (z-score across states, within day), n=597 neurons from 4 mice.

F. Quantitative analyses of cue-responsive neurons. *Left*: fraction of all recorded neurons (n=597 neurons from 4 mice) responsive to each visual cue. *Right*: average response magnitude. **$p \leq 9 \times 10^{-4}$, n.s.: not significant (p=0.07), *p=0.01, Kruskal-Wallis test. Pairwise comparisons ('Quenched+SFO^{GLUT} stim.'): p≤0.01, except aversive cue vs. neutral cue (p≥0.57). Pairwise comparisons ('Quenched+SFO^{GLUT} stim.' vs. 'Quenched'): **p≤0.03 for all 3 cues, Mann-Whitney test (neurons responding to the water, aversive and neutral cues: suppressed: n=75, 39 and 40, respectively; activated: n=49, 8, and 8; from 4 mice).

G. Heatmap of all water cue-responsive neurons during the 3 experimental conditions.

H. Fraction of neurons that were similarly responsive across pairs of conditions (n=194 neurons from 4 mice). Values are mean±s.e.m. across mice.

Author Manuscript Author Manuscript Author Manuscript Author Manuscript

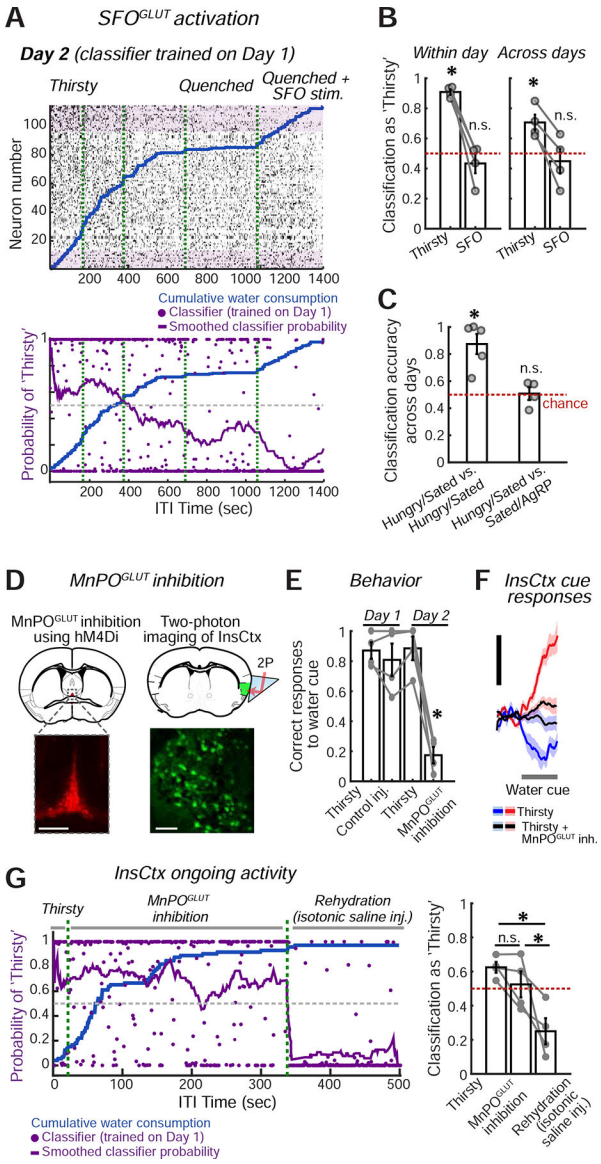

Figure 6: Manipulations of Hypothalamic Hunger and Thirst Neurons Do Not Affect InsCtx Ongoing Activity

A. *Top*: example ongoing activity of an InsCtx population on the second day of the experiment. *Bottom*: classification of all time points. Classifier was trained on the previous day's ongoing activity. Green dashed lines: separation between consecutive 30 min imaging sessions.

B. Summary of classification of ongoing activity during 'Thirsty' and 'Quenched+SFO^{GLUT} activation' across mice. *p≤0.014; ns: not significant, p≥0.38; t-test vs. chance (n=4 mice).

C. Summary of classification of ongoing activity during 'Hungry' and 'Sated+AgRP activation' across mice. 'Hungry/Sated vs. Hungry/Sated': classifier trained on Hungry vs. Sated on Day 1 and tested on Hungry vs. Sated on Day 2. 'Hungry/Sated vs. Sated/AgRP': classifier trained on Hungry vs. Sated on Day 1 and tested on Sated vs. 'Sated+AgRP activation' on Day 2. *p≤0.007; n.s.: not significant, p≥0.87, t-test vs. chance (n=4 mice).

Author Manuscript Author Manuscript Author Manuscript Author Manuscript

D. Experimental approach for chemogenetic inhibition of MnPO^{GLUT} neurons (*top left*), while imaging InsCtx (*top right*). *Bottom left*: image of MnPO showing hM4Di-mCherry expression. Scale bar: 200 μm. *Bottom right*: two-photon image of InsCtx during MnPO^{GLUT} inhibition. Scale bar: 100 μm.

E. Summary of behavior across mice (n=4). Correct water cue responses across conditions: $p=6.6\times10^{-5}$ (one-way ANOVA), MnPO^{GLUT} inhibition vs. all other conditions: *p<0.0005 (paired t-test). All other comparisons were not significant. All tests include Holm-Bonferroni correction for multiple comparisons.

F. Average population responses of all imaged neurons to the water cue during the different conditions. Scale bars: 0.5 normalized ΔF/F (z-score across states, within day).

G. Ongoing activity across ‘Thirsty’, ‘Thirsty + MnPO^{GLUT} inh.’, and ‘Rehydration’ conditions. *Left*: classification of all time points. Classifier was trained on the previous day’s ongoing activity. Green dashed lines separate consecutive 15 or 30 min imaging sessions. *Right*: summary of classification of ongoing activity across conditions. ‘Thirsty’ vs. ‘Thirsty + MnPO^{GLUT} inh.’: p=0.08; ‘Thirsty’ vs. ‘Rehydration’: p=0.015; ‘Thirsty + MnPO^{GLUT} inh.’ vs. ‘Rehydration’: p=0.04 (paired t-test). All tests include Holm-Bonferroni correction for multiple comparisons (n=4 mice). Values are mean±s.e.m. across mice.

Author Manuscript Author Manuscript Author Manuscript Author Manuscript

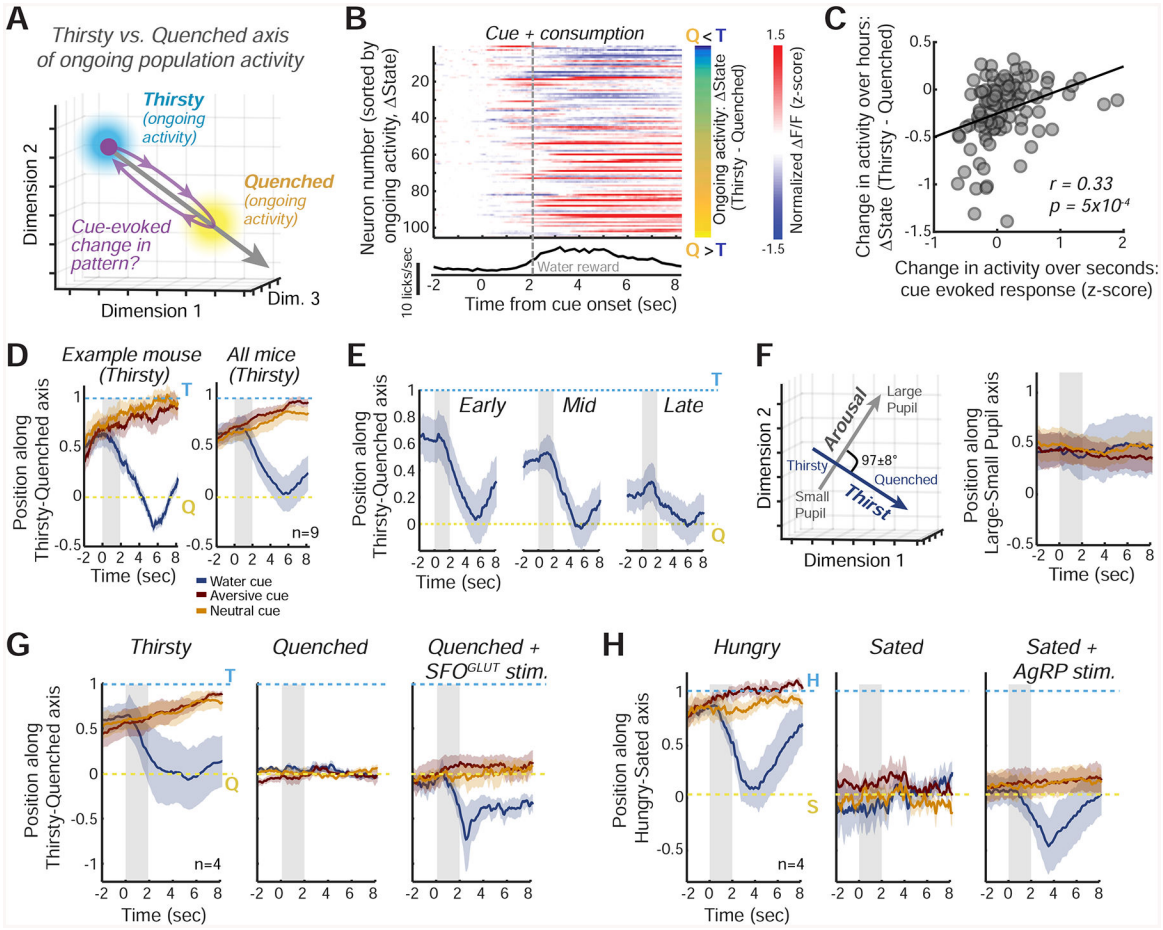

Figure 7: InsCtx Population Activity During Water/Food Cues and Consumption Transiently Resembles a Future Satiety State

A. Schematic of the approach for assessing changes in the similarity of *cue-evoked* InsCtx activity patterns to *ongoing* activity patterns during Thirsty and Quenched states. See Fig. S6C for further details.

B. *Top*: example session with InsCtx neuronal responses to the water cue and subsequent water consumption ('cue + consumption', change from baseline activity). Activity was sorted by the difference in *ongoing* activity between Thirsty (T) and Quenched (Q) states (ΔState, *right*, values: −0.3 to 1.4). *Bottom*: average licking.

C. Correlation between InsCtx neurons' 'cue + consumption' evoked responses and their changes in ongoing activity between Thirsty and Quenched states (ΔState), for the example in **B**.

D. *Left*: example pattern similarity of InsCtx peri-cue population activity in the Thirsty state to ongoing activity in the Thirsty vs. Quenched states. Mean±s.e.m. across 45 presentations of each cue. *Right*: mean±s.e.m across 9 FOVs from 7 mice. Gray shaded areas: cue period.

E. Pattern similarity of InsCtx peri-cue population activity during gradual quenching to ongoing activity in the Thirsty vs. Quenched states. Gray shaded areas: cue period.

F. Population activity along the Large Pupil vs. Small Pupil axis (arousal), in comparison with the Thirsty vs. Quenched axis (physiological state, see also **D**, *right*). *Left*: these axes are approximately orthogonal (mean angle: 97±8°). *Right*: pattern similarity of InsCtx peri-

Author Manuscript Author Manuscript Author Manuscript Author Manuscript

cue population activity during a thirsty state to ongoing activity along the Large Pupil vs. Small Pupil axis. Mean±s.e.m across 9 FOVs from 7 mice. Values of 1 and 0 correspond to mean ongoing activity patterns in epochs with large and small pupil, respectively.

G. Pattern similarity during water cue trials in 'Thirsty', 'Quenched', and 'Quenched +SFO^{GLUT} activation' states. Gray shaded areas: cue period. Mean±s.e.m across 4 mice.

H. Similar to **G**, but for food cues across 'Hungry', 'Sated', and 'Sated+AgRP activation' states. Gray shaded areas: cue period. H: hungry; S: sated. Mean±s.e.m across 4 mice.

Author Manuscript Author Manuscript Author Manuscript Author Manuscript

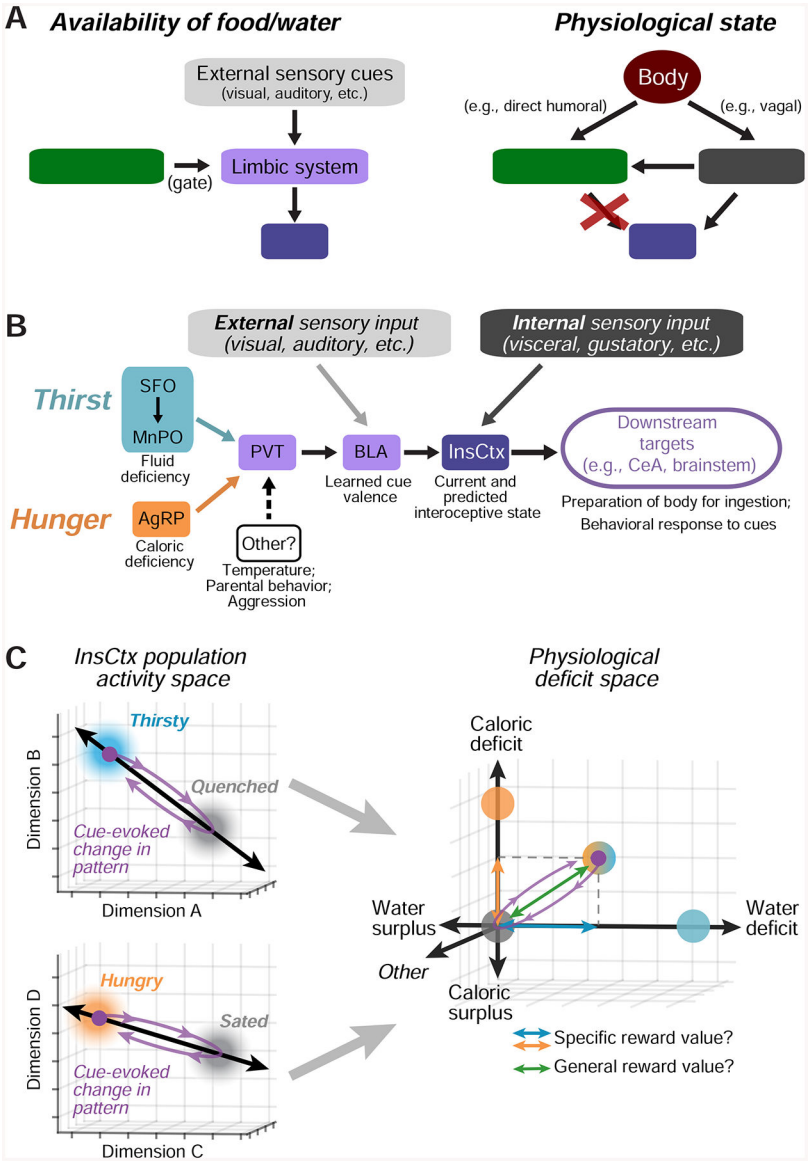

Figure 8: Models of InsCtx Representations of Current and Future Physiological States

A.Models of the potential mechanisms generating representations of predictive cues (*left*) and current physiological states (*right*) in InsCtx. Arrows represent interactions, not monosynaptic connectivity. Red 'X': manipulations of hypothalamic hunger/thirst neurons did not affect InsCtx representations of physiological states (Fig. 6). See Discussion.

B. Model of the specific limbic pathway to InsCtx onto which hypothalamic hunger and thirst neurons converge. Other neurons that drive distinct motivations also anatomically converge in PVT. See Discussion.

C. Conceptual model of how each of multiple need states may be represented in InsCtx by distinct activity patterns across intermingled neurons, and therefore along distinct axes in the space of population activity. The activity in a replete state (eucaloric, euhydrated, euthermic, etc.) may be a "set point". In this example, a cue predicting liquid food should supply both

water and calories to relieve both thirst and hunger, and thereby drive movement along both axes. See Discussion.

Author Manuscript Author Manuscript Author Manuscript Author Manuscript

Author Manuscript Author Manuscript Author Manuscript Author Manuscript

Key Resources Table

REAGENT or RESOURCE	SOURCE	IDENTIFIER
Antibodies		
Chicken anti-GFP	Invitrogen	Cat #: A10262; RRID: AB_2534023
Rat anti-mCherry	Invitrogen	Cat #: M11217; RRID: AB_2536611
Bacterial and Virus Strains		
AAV1-hSyn-GCaMP6f	Penn Vector Core	Addgene 100837
AAV1-hSyn-GCaMP6s	Penn Vector Core	Addgene 100843
AAV8-hSyn-DIO-hM3Dq-mCherry	UNC Vector Core	Addgene 44361
AAV8-hSyn-DIO-hM4Di-mCherry	UNC Vector Core	Addgene 44362
AAV1-DIO-ChR2(H134R)-YFP	Penn Vector Core	Addgene 20298
AAV8-FLEX-TVA-mCherry	UNC Vector Core	Addgene 38044
SADΔG–EGFP (EnvA) rabies	Salk Gene Transfer Targeting and Therapeutics Core	Addgene 32635
AAV8-CaMKII-hM3Dq-mCherry	Addgene	Addgene 50476
Chemicals, Peptides, and Recombinant Proteins		
Clozapine-N-Oxide (CNO)	NIMH Drug Supply	Program Cat# C-929
Compound 21 (C21)	Tocris	6422
CNQX	Tocris	Cat# 0190
D-AP5	Tocris	Cat# 0106
Kynurenic Acid	Sigma-Aldrich	Cat# K3375–5G
Picrotoxin	Tocris	Cat# 1128
Bicuculline	Tocris	Cat# 2503
TTX	Tocris	Cat# 1069
4-AP	Sigma-Aldrich	Cat# A78403
Cholera Toxin B Subunit B (Recombinant), Alexa Fluor 555 Conjugate	Thermo Fisher	Cat# 34776
Experimental Models: Organisms/Strains		
Mouse: C57BL/6J	The Jackson Laboratory	RRID: IMSR_JAX:000664
Mouse: Nos1-Cre knockin (B6.129-Nos1tm1(cre)Mgmj/J)	The Jackson Laboratory	Strain# 017526; RRID: IMSR_JAX:017526
Mouse: vGlut2-ires-Cre (B6J.129S6(FVB)-Slc17a6tm2(cre)Lowl/MwarJ)	The Jackson Laboratory	Strain# 028863; RRID:IMSR_JAX:028863
Software and Algorithms		
MATLAB R2015b, 2019a	Mathworks	https://www.mathworks.com/products/matlab.html; RRID: SCR_001622
MonkeyLogic	Asaad and Eskandar, 2008	http://www.brown.edu/Research/monkeylogic/
MonkeyLogic2	NIMH	https://monkeylogic.nimh.nih.gov/
Scanbox	Neurolabware	https://scanbox.org/
PCA/ICA neuron identification	Mukamel et al., 2009	https://github.com/mukamel-lab/CellSort
Glmnet	Friedman et al., 2010	https://web.stanford.edu/~hastie/glmnet_matlab/
ImageJ 1.49t	NIH	https://imagej.nih.gov/ij/; RRID: SCR_003070